EFDA–JET–R(10)02

K.D. Lawson, J. Zacks, I.H. Coffey, K.M. Aggarwal, F.P. Keenan
and JET-EFDA Contributors

Comparison of Modelled C VUV Line Intensity Ratios with Observations of the Emission from the JET Plasma SOL-II

Comparison of Modelled C VUV Line Intensity Ratios with Observations of the Emission from the JET Plasma SOL-II

K.D. Lawson[1], J. Zacks[2], I.H. Coffey[2], K.M. Aggarwal[2], F.P. Keenan[2]
and JET-EFDA Contributors*

[1]*National Research and Development Institute for Cryogenics and Isotopic Technologies*
[2]*Astrophysics Research Center, School of Mathematics and Physics, Queen's University, Belfast, BT7 1NN, Northern Ireland, UK*
** See annex of F. Romanelli et al, "Overview of JET Results", (Proc. 22 nd IAEA Fusion Energy Conference, Geneva, Switzerland (2008)).*

Comparison of modelled C VUV line intensity ratios with observations of the emission from the JET plasma SOL - II

K D Lawson[1], J Zacks[2], I H Coffey[2], K M Aggarwal[2], F P Keenan[2] & JET-EFDA Contributors*

JET-EFDA, Culham Science Centre, Abingdon, OX14 3DB, UK
[1] *Euratom/UKAEA Fusion Association, Culham Science Centre, Abingdon, OX14 3DB, UK*
[2] *Astrophysics Research Center, School of Mathematics and Physics, Queen's University, Belfast, BT7 1NN, Northern Ireland, UK*

Abstract

Lawson *et al*. (2009a) gave details of a comparison between measured and modelled or theoretical C II to C IV line intensity ratios of emission from the edge of the JET plasma. The radiation was recorded with two spectrometers that observe the VUV and XUV emission from the plasma along a horizontal line-of-sight. Line intensity ratios were calculated using a collisional-radiative model and discrepancies were found with the measured values. However, for the VUV instrument a very accurate sensitivity calibration was only available at shorter wavelengths. At longer wavelengths the accuracy of the sensitivity calibration was poorer, limiting the usefulness of some of the measurements. In addition, the paper investigated various possible causes of the observed discrepancies, but no satisfactory explanation was found.

In the present paper, the discrepancies found for the C IV ionization stage measured with a VUV spectrometer having a vertical line-of-sight that views the Scrape-off-Layer (SOL) above the throat of the outer divertor are detailed. This spectrometer, which has a wavelength range of 140Å to 443Å, is ideal for observing the C IV ionization stage and has the advantage of an accurate sensitivity calibration throughout its wavelength range. It is noted that measurements with this instrument of the emission from the divertor plasma show agreement with theory to within the experimental accuracy (Lawson *et al*., 2010).

Two further possible explanations of the discrepancy are investigated here. These are differences resulting from the line-of-sight averaging of the measurements across a plasma region with steep gradients and the possibility of non-Maxwellian electron energy distributions affecting the electron collisional excitation rates. The results of these further studies are presented.

1. Introduction

The simplest and most direct way of testing the models and atomic data used to interpret passive line emission from a plasma is to compare ratios of theoretical intensities of spectral lines emitted from the same ionization stage with their measurements. The use of such line intensity ratios avoids the need to determine the emitting plasma volume, some parameters such as the electron density and an absolute sensitivity calibration for the spectrometer used, thus making the analysis more reliable. This analysis was undertaken for the C II to C IV emission from the edge of the JET plasma and has been reported by Lawson *et al*. (2009a), referred to as Paper I. The most detailed study was carried out for the C IV ionization stage.

Part of the interest in the analysis is that C line intensity ratios allow the sensitivity calibration of the JET VUV SPRED survey spectrometer, KT2, to be extended to longer

wavelengths. A short wavelength calibration had been determined using Na- and Li-like metal line intensity ratios (Lawson *et al*. 2009b), for which agreement to within the measurement accuracy of ~6% had been found; this resulted in a particularly accurate calibration, ~±10%. In contrast, discrepancies of ~45% were found when C line intensity ratios were used to extend the calibration to longer wavelengths. Paper I provides details of these discrepancies and investigates some possible causes.

The commonest cause of errors in the VUV spectral region is line blending and a thorough check of possible blends was made. The validity of the normally used steady-state assumption was also checked and the importance of additional populating mechanisms such as recombination, both charge exchange and free electron, was investigated. No satisfactory explanation of the discrepancies was found.

In the present paper, discrepancies between the theoretical line intensity ratios and measurements made using the divertor viewing double SPRED spectrometer, KT7, are described. This instrument, details of which are given in section 2, is positioned on top of the machine and can be tilted poloidally so as to view anywhere between the inner divertor plasma and the SOL above the throat of the outer divertor. One of its detectors has a wavelength range of 140Å to 443Å and is ideal for observing the C IV spectrum. Furthermore, this detector has a very accurate relative sensitivity calibration, throughout the wavelength range of the C IV spectrum. With a view into the divertor good agreement is found between the measured and modelled line intensity ratios (Lawson *et al*. 2010), thus confirming the expected accuracy of the atomic data and removing any question about instrumental effects causing the discrepancy. When the spectrometer is tilted a few degrees to observe the SOL, significant discrepancies are found, which are described in section 3. The collisional radiative model used has been explained in section 3 of Paper I. Two further possible causes of the discrepancies are discussed in section 4. Section 4a deals with the possibility of non-Maxwellian electron energy distributions in the plasma edge affecting the electron collisional excitation rates and, consequently, the measured line ratios. In section 4b, discrepancies due to line-of-sight averaging in regions of steep gradients as are expected in the plasma edge are investigated. The conclusions are given in section 5.

2. Experimental Arrangement

a. XUV/VUV survey spectrometer

The XUV/VUV spectrometer viewing the JET divertor, KT7, (Wolf *et al*., 1995) consists of three instruments, two SPRED spectrometers (Fonck *et al*. 1982) and a Schwob-Fraenkel SOXMOS instrument (Schwob *et al*., 1987). It has a vertical line-of-sight looking from the top of the machine towards the JET divertor, as illustrated in figure 1. The diagnostic can be tilted poloidally allowing the line-of-sight to view anywhere from the inner divertor through to the SOL above the throat of the outer divertor. The Na- and Li-like data used to obtain the sensitivity calibration (section 2b) were recorded with this outermost line-of-sight. As can be seen in figure 1, this line-of-sight passes through the core plasma. With a view into the divertor, the radiation from the lower ionization stages of C is dominated by emission from the divertor box .

The SPREDs are enclosed in stainless steel shielding to reduce noise due to both neutrons and γ-rays, with 15cm of shielding between the plasma and detectors and 5cm thickness at the back and sides. The detectors are microchannel plate (MCP) / phosphor combinations which are coupled to a Reticon photodiode array via a fibre optic bundle. It is the interaction of the neutrons and γ-rays with the MCP, with its high gain, that is of most concern. A shielding of

15cm of steel was expected to reduce the 2.5MeV neutron flux by a factor of ~8 and that of 8MeV γ-rays by a factor of ~17. Comparisons were made shortly after the double SPRED was first commissioned with the JET SPRED survey spectrometer, KT2, which is unshielded. These suggested that the background due to nuclear reaction products was a factor ~7 lower in the double SPRED than the unshielded instrument.

Originally, 0.5mm thick MCPs were installed in the double SPRED, but these were found to be very fragile. In 1998 they were replaced with MCPs that were 1mm thick, which also gave increased sensitivity. The MCPs have a CuI coating to enhance the electron emission. The double SPRED uses toroidal holographic gratings, that with the higher resolution (in KT7/2) having a ruling density of 2105g.mm^{-1}, the other (in KT7/1) 450g.mm^{-1}. Both have extended and shifted spectral ranges compared to the standard SPREDs. KT7/2 observes the wavelength range 140Å to 443Å with a spectral resolution of ~1Å. Normally the gratings used in the SPREDs enhance the first and third spectral orders; however, in the present case the second spectral order is weakly detected, but with a greater intensity than the third.

Both SPREDs have 2048 pixels, although the KT7/2 detector developed a fault in which adjacent pairs of pixels output the same reading, essentially reducing the useful number of pixels to 1024. A simple and reliable line integration method was employed, in which a fixed number of pixels on either side of the line centre define an integration range and the background to be subtracted. This method takes advantage of the similarity of the spectral line profile throughout the wavelength range of the instrument. The integration is performed using Simpson's rule. With 2048 pixels a ±5 pixel integration range is preferred. However, with only 1024 pixels a ±3 pixel range is ideal for intense lines, but is too wide for weak lines. For intense lines this range covers almost the full line profile, whereas a ±2 pixel range is assessed to be too narrow to ensure the most accurate integration for these lines. In the profile of weak lines, the third pixel on either side of the line centre tends to be absorbed into the background and therefore will not be reliable. Consequently, a ±2 pixel range is the maximum that can be used. The calibration is derived using intense lines for which the ±3 pixel range is appropriate. In order to measure weak lines the ratio of the ±3 to ±2 pixel integrations is also required, this being described by Lawson *et al*. (2009c).

The design of the diagnostic is particularly robust making the spectrometer very stable mechanically. This is advantageous in running the instrument on JET with its long period of operations during which there is limited access to the machine.

b. Sensitivity calibration

An essential prerequisite to this study is the provision of a relative sensitivity calibration for the wavelength range of interest. This was achieved for the higher resolution detector of the double SPRED, KT7/2, by using a series of Na- and Li-like doublet line intensity ratios, which resulted in an exceptionally accurate relative calibration. The same method had previously been used for the short wavelength end of KT2 (Lawson *et al*. 2009b).

The Na- and Li-like doublets of a number of intrinsic metallic impurities are observed throughout the spectral range of KT7/2. They correspond to the $2p^6 3s\ ^2S_{1/2} - 2p^6 3p\ ^2P_{1/2,3/2}$ and $1s^2 2s\ ^2S_{1/2} - 1s^2 2p\ ^2P_{1/2,3/2}$ transitions, respectively. In addition, the noble gases Ar and Kr can be introduced into the plasma by gas puffing, these elements having a similar doublet structure. Figure 2 shows the spectrum for pulse 67966, averaged between times 9.3 and 9.4s, with doublets belonging to Cr, Fe, Ni and Cu observed. In addition one of the Mn XXIII lines and the Ar XVI and Cr XIV doublets appear weakly in this spectrum. In contrast, the 192.0Å line of the Fe XXIV doublet is saturated and the Fe XXIII 132.9Å line, which is expected to be of similar intensity, can be seen weakly in the second and third orders. A comparison of the theoretical and measured doublet line intensity ratios yields the ratio of sensitivities at the

doublet wavelengths. Neighbouring doublets can then be used to extend the calibration to either shorter or longer wavelengths.

These intensity ratios are ideal for determining the sensitivity calibration, since they are found to be independent of n_e and are only very weakly dependent on T_e. They are modelled using a collisional-radiative model, already described in Paper I. Ratios were calculated at a temperature equal to the ionization potential and at half and double this temperature. Since the ratios differed by less than 2% over this wide temperature range, the values for the central temperatures were adopted. Sampson *et al*. (1990) and Zhang *et al*. (1990) have provided relativistic distorted wave calculations of the electron collisional excitation rates for, respectively, the Na- and Li-like ionization stages for a wide range of elements. There are also R-matrix calculations for Ar XVI and Fe XXIV by Whiteford *et al*. (2002). Comparisons of the line intensity ratios modelled using the different electron rates, calculated with the ADAS atomic data package (Summers, 2004), show agreement to within ~1%. Interpolated values were obtained for those elements for which there are no published data and an adjustment was made to account for the marginally higher (~1%) Ar XVI and Fe XXIV R-matrix excitation rates. It is expected that the derived line intensity ratios are accurate to a few per cent. In all, ten doublet ratios were used, their wavelengths extending from 153.5Å up to 412.0Å, almost the complete range of the higher resolution detector.

The detailed analysis of the Na- and Li-like doublets, described by Lawson *et al*. (2009c), suggests a particularly good accuracy for the calibration more typical of the visible spectral region rather than the VUV. Nevertheless, given the step-by-step procedure for its derivation, it is important to have confirmation of the calibration to ensure that there is no cumulative error. This can be provided by the C IV line intensity ratios emitted from the divertor plasma. Again, theoretical and measured line intensity ratios are compared. However, in this case, the model is more complicated, since the C IV ratios depend on electron temperature and recombination (particularly charge exchange recombination) must be considered as a populating mechanism. Six C IV lines were used in the analysis. They are listed in table 1 and can be seen in figure 3, which shows the spectrum of pulse 69931 recorded between times 2.3 and 2.6s. A check was made as to the effect of the C III line at 386.2Å on the integration of the 384.1Å line; this was found to be at most 2%. The three lowest wavelength lines are comparatively weak, a ±2 pixel range being used for their integration. Line intensity ratios of emission from the divertor were measured during the Ohmic phase in 86 pulses and the additionally heated phase in 165 pulses. In applying the collisional-radiative model, the differences between the measured and theoretical ratios were minimized. Further information about this procedure is given by Lawson *et al*. (2009c) .

Table 1. C IV lines used in the analysis

Wavelength (Å)	Transition	Integration range	Blends
244.9	$1s^2 2s\ ^2S_{1/2} - 1s^2 4p\ ^2P_{1/2,3/2}$	±2	
289.2	$1s^2 2p\ ^2P_{1/2,3/2} - 1s^2 4d\ ^2D_{3/2,5/2}$	±2	
296.9	$1s^2 2p\ ^2P_{1/2,3/2} - 1s^2 4s\ ^2S_{1/2}$	±2	
312.4	$1s^2 2s\ ^2S_{1/2} - 1s^2 3p\ ^2P_{1/2,3/2}$	±3	
384.1	$1s^2 2p\ ^2P_{1/2,3/2} - 1s^2 3d\ ^2D_{3/2,5/2}$	±3	CIII, 386.2Å
419.6	$1s^2 2p\ ^2P_{1/2,3/2} - 1s^2 3s\ ^2S_{1/2}$	±3	

It was clear from the analysis that overall the measured and theoretical C IV divertor line intensity ratios were consistent. Differences for the individual line intensity ratios averaged

over both databases are less than 9%. An exception was the 384.1Å/312.4Å ratio, which had a difference of 16.5%, although this was in part due to the deviation of the Ar XVI 389.1Å point by ~7% from the general trend of the calibration. Given this consistency, the most accurate calibration will be obtained by combining the Na- and Li-like results with those of C IV, supposing that differences in the C IV line ratios are due to discrepancies in the calibration. A second order polynomial fit was made to both sets of data. Since the measured C IV ratios depend on the calibration it was necessary to repeat the fits, two iterations being required before subsequent changes in the calibration were less than 1%. Inclusion of the C IV data led to changes in the calibration of at most 13%, this being at a wavelength of 419.6Å, -5% at 384.1Å and less than 2% at shorter wavelengths. The relative inverse sensitivity calibration and final polynomial fit are shown in figure 4, the sensitivity being normalized to that at 312.4Å. This procedure is justified in that the resulting polynomial fit is close to a straight line in logarithmic space, falling between the Ar XVI 389.1Å and C IV 384.1Å points. The resulting calibration is expected to be accurate to ±10% throughout the wavelength range that includes the C IV lines.

3. Experimental Results

Paper I describes the comparison of theoretical C II to C IV line intensity ratios with measurements made with the JET VUV SPRED survey spectrometer, KT2, and the XUV Schwob-Fraenkel spectrometer, KT4, both of which have horizontal lines-of-sight close to the vessel midplane. The measurements were made during the limiter phase of the discharges when the C signals are intense and when minimal contamination of the spectrum from other elements is expected, these two factors combining to give the most reliable measurements possible.

The most detailed study was made for C IV. In order to characterize the discrepancies for this ionization stage, they are somewhat arbitrarily defined as the measured intensity ratio divided by the theoretical ratio calculated for the temperature found from the 312.4Å/289.2Å line ratio,

$$d(T_e) = \frac{R_m}{R_t}, \tag{1}$$

where R_m is the measured intensity ratio and R_t the theoretical ratio. The 312.4Å/289.2Å line ratio was chosen for the temperature determination, both because of its temperature sensitivity and because a reliable sensitivity calibration is available for these wavelengths. It is noted that in this calculation recombination is not included, since it was shown in Paper I that recombination, either free electron or charge exchange, could not explain the observed discrepancies. For ease of comparison the discrepancies plotted against the 312.4Å/289.2Å temperature found for five C IV line ratios, 419.6Å/312.4Å, 419.6Å/289.2Å, 384.1Å/312.4Å, 296.9Å/312.4Å and 244.9Å/312.4Å (figures 12 to 16 of Paper I) are reproduced here as figures 5 to 9. Paper I also demonstrated that there was disagreement between the temperature measurements obtained from different line ratios. Hence, there is uncertainty regarding the accuracy of the 312.4Å/289.2Å measurement of temperature.

A limitation of the KT2 and KT4 results was that an accurate sensitivity calibration for the KT2 spectrometer was only available for the short wavelength end of its spectral range, that for longer wavelengths being less certain. All the C II lines observed, most of the C III lines and even the longest two C IV lines at 384.1Å and 419.6Å fell in this longer wavelength range. On the other hand, the very accurate sensitivity calibration available for KT7/2, whose wavelength range is ideally suited for observing the same C IV lines as analyzed in Paper I, allows accurately calibrated measurements of these lines. With a view into the JET divertor,

agreement between the measured and theoretical line intensity ratios to within measurement uncertainties (~±10%) is found (Lawson *et al*., 2010). However, when the spectrometer is tilted to view the SOL above the outer throat of the divertor, significant discrepancies are found with the same instrumental set-up and performing the same analysis. That agreement was found for the divertor plasma emission confirms a conclusion of Paper I that the discrepancies are not due to inaccuracies in the atomic data and also shows that they cannot be explained by some instrumental effect. A database of C IV measurements recorded by KT7/2 with a view of the SOL is presented here; the very accurate and complete sensitivity calibration makes these measurements of particular value.

The KT7/2 line-of-sight into the SOL is nevertheless close enough to the divertor for the C emission during the X-point phase to be more intense than during the limiter phase, which is not necessarily the case with the C emission along a horizontal line-of-sight. Consequently, since three of the lines being observed are weak, the X-point phase was preferred for the KT7/2 measurements. Nevertheless, to minimize the contamination of the spectrum by other impurity lines the Ohmic phase is chosen. This phase also has the advantage of being the simplest, avoiding possible variations in the plasma edge and, hence, C IV emission due to the type of additional heating used or its input power, etc. A database of 71 Ohmic measurements has been compiled. As in the databases used in Paper I and by Lawson *et al*. (2010) no particular selection of pulses was made, apart from avoiding pulses with significant He or higher Z impurity gas puffing. Again, it is expected that this should make the results more general than if a particular experiment was studied. The discrepancies for these data are plotted against the 312.4Å/289.2Å temperature in figures 10 to 14. It can be seen that these temperatures are lower than might be expected, for example, significantly lower than found by Lawson *et al*. (2010) for the C IV emitting divertor plasma region. For the Ohmic database this varied between 17 and 48eV. The low temperatures are themselves a clear indication that the model being used is incomplete. However, to make sure that it is not just a difficulty with the 312.4Å/289.2Å line ratio, which is being used for the temperature measurements, the temperatures were rescaled to match the divertor temperatures. As can be seen in figures 15 to 19, there are still significant discrepancies compared with the experimental accuracy of ~±10%.

In these diagrams, the temperature is a useful means of separating and displaying the data points, although it should be remembered that they also affect the magnitude of the discrepancy, the theoretical ratios being calculated at the 312.4Å/289.2Å temperature. Consequently, the differences in the temperature dependence of the discrepancies between the three sets of data, figures 5 to 9, figures 10 to14 and figures 15 to 19, is not surprising. Straight line fits have been made to the data in figures 10 to 19, as has been done for figures 5 to 9.

4. Discussion

a. Non-Maxwellian electron energy distributions

The effective collision strengths for electron collisional excitation, which in turn give the electron collisional rates, are derived from the collision strengths by averaging over the electron energy distribution. Although a fluid analysis, in which the particle energy distributions are taken to be Maxwellian, is normally found to be appropriate for the plasma edge, the fluid approximation can be marginal, this depending on the temperature and density of the edge plasma. Consequently, it was thought worthwhile to investigate the effect of

variations in the electron energy distribution from a Maxwellian distribution to see if this could explain the observed discrepancies.

The electron collisional rate for a transition from state i to j, q_{ij}, is derived from the collision strength, $\Omega_{ij}(E_j)$, calculated as a function of the electron impact energy relative to the final state j of the transition E_j,

$$q_{ij} = 2\alpha c a_0^2 \left(\frac{\pi I_H}{T_e}\right)^{\frac{1}{2}} \frac{\gamma_{ij}}{\varpi_i} \exp\left(\frac{-E_{ij}}{kT_e}\right).$$

If the electron energy distribution is Maxwellian, then the effective collision strength

$$\gamma_{ij} = \int_0^\infty \Omega_{ij} \exp\left(-\frac{E_j}{kT_e}\right) d\left(\frac{E_j}{kT_e}\right).$$

In these equations α is the fine structure constant, c the velocity of light, a_0 the Bohr radius, I_H the ionization potential of H, E_{ij} is the transition energy, k the Boltzmann constant and ω_i the statistical weight of the initial state. However, if the electron energy distribution is non-Maxwellian, the concept of electron temperature, T_e, has no meaning. Instead, the electron collisional rate is defined as

$$q_{ij} = \frac{\pi\alpha c a_0^2}{\varpi_i} (I_H)^{\frac{1}{2}} \int_0^\infty \frac{g(E_i)}{E_i^{0.5}} \Omega_{ij}\, dE_i \,. \qquad (2)$$

Here the electron energy distribution, g, is defined as a function of the electron impact energy E_i.

Table 2. Energies of the upper levels of the C IV transitions

Distribution curve index	Energy level	NIST energy (Ry)	GRASP energy (Ry)	Energy vector index
0	$1s^2 3s\ ^2S_{1/2}$	2.7598	2.7533	550
1	$1s^2 3p\ ^2P_{1/2,3/2}$	2.9165, 2.9168	2.9116,2.9119	582
2	$1s^2 3d\ ^2D_{3/2,5/2}$	2.9605,2.9606	2.9529,2.9529	590
3	$1s^2 4s\ ^2S_{1/2}$	3.6574	3.6496	729
4	$1s^2 4p\ ^2P_{1/2,3/2}$	3.7208,3.7209	3.7137,3.7138	742
5	$1s^2 4d\ ^2D_{3/2,5/2}$	3.7393,3.7393	3.7311,3.7311	746
6				2000

In order to test non-Maxwellian electron energy distributions, the distribution was divided into sections bounded by the energies of the upper levels of the observed C IV transitions, which are listed in table 2. This allows the non-Maxwellian distribution to be investigated in the simplest way possible given the available measurements. The electron energies in the section with an index 0 were less than 2.75Ry (1Ry = 13.6058eV) and are too small to make any contribution to the populations of the upper levels of the C IV transitions of interest. The section with an index 1 contains electrons with sufficient energy to contribute to the upper level of the 419.6Å transition, that with an index 2 to the 419.6Å and 312.4Å transitions and so on. Different sections of the distribution could then be varied and the electron excitation rate calculated using equation (2). The integration is performed numerically, with an energy resolution of 0.005Ry up to an energy of 10Ry, using the full dataset of collision strengths that gave the results presented by Aggarwal and Keenan (2004). Checks were made to

determine the minimum energy resolution and energy range required. Increasing the energy resolution from 0.05 to 0.005Ry made little difference (~0.01%) to the integration of a test Maxwellian distribution, although resulted in more points falling within each section of the distribution curve. In contrast, a significant difference was found as the limits of the integration were increased. It was necessary to integrate up to 10Ry to ensure better than 1% agreement with the integrated test Maxwellian curve, although doubling this range then made little (~0.1%) difference.

For simplicity the rates were input into a low density limit model. In this approximation, the steady state rate equation for n_i, the population density of the ith level,

$$\frac{dn_i}{dt} = n_e \sum_{j \neq i} n_j q_{ji} - n_e \sum_{j \neq i} n_i q_{ij} + \sum_{j>i} n_j A_{ji} - \sum_{j<i} n_i A_{ij} = 0 ,$$

is rearranged assuming that the only significant collisional excitation or deexcitation is excitation from the ground level, g, to give

$$\frac{n_i}{n_e n_g} = \frac{1}{\sum_{j<i} A_{ij}} \left(q_{gi} + \sum_{j>i} \frac{n_j}{n_e n_g} A_{ji} \right).$$

The density ratio $n_j/n_e n_g$ is calculated in a similar way. The intensity of a line denoted 1 is given in terms of the ADAS Photon Emission Coefficients (PECs) (Summers, 2004) by

$$I_1 = n_e n_g \varepsilon_1^{exc} + n_D n_{g+1} \varepsilon_1^{cx} ,$$

where the excitation PEC is

$$\varepsilon_1^{exc} = \frac{A_1}{\sum_{j<i} A_{ij}} \left(q_{gi} + \sum_{j>i} \frac{n_j}{n_e n_g} A_{ji} \right)$$

and ε^{cx} is the corresponding charge exchange PEC. In terms of the PECs, the line intensity ratio between lines 1 and 2 becomes

$$\frac{I_1}{I_2} = \frac{\varepsilon_1^{exc} + \dfrac{n_D n_{g+1}}{n_e n_g} \varepsilon_1^{cx}}{\varepsilon_2^{exc} + \dfrac{n_D n_{g+1}}{n_e n_g} \varepsilon_2^{cx}} .$$

Lawson *et al*. (2010) showed the importance of charge exchange as a populating mechanism, but that free electron recombination is of less importance. Consequently, a charge exchange term is included, but not the free electron recombination PEC. The charge exchange data was taken from ADAS, being compiled from various sources by Maggi (1996). Checks were made to ensure that the use of the low density limit approximation did not affect the accuracy of the results, agreement for the test Maxwellian case between the line intensity ratios calculated using this approximation being within 1% of the full solution.

The measured data given in section 3 is used for this investigation. This is both because the accurate sensitivity calibration of the spectrometer makes this the most reliable dataset and because the magnitude of the discrepancy is larger than for the database presented in Paper I. Indeed, it is only possible to give a conclusive answer because of the wider range of

the discrepancies in this database. If the discrepancies are due to a non-Maxwellian electron energy distribution it should be possible to reproduce the straight line fits to these data by varying different sections of the distribution curve. Five line intensity ratios were used, ratios of the lines listed in table 1 being taken with the 312.4Å line. Two 'temperatures', 6.5 and 10.5eV, are chosen and the modelled intensity ratios found. As already noted the concept of temperature is no longer valid in the case of a non-Maxwellian electron energy distribution

Table 3. Results of the non-Maxwellian analysis, listing multiplication factors for the electron energy distribution curve and the charge exchange densities ratio.

Sections varied	Nominal 'T_e' (eV)	Multiplication factors for the sections of the electron energy distribution curve						CX densities ratio	RMS fractional difference
		1	2	3	4	5	6		
123	6.5	0.0	4.011	0.236	1.0	1.0	1.0	0.0006	0.210
123	10.5	0.0	0.673	1.338	1.0	1.0	1.0	0.0030	0.038
124	6.5	0.0	10.00	1.0	1.018	1.0	1.0	0.0020	0.220
124	10.5	0.0	0.351	1.0	0.524	1.0	1.0	0.0014	0.034
125	6.5	0.0	10.00	1.0	1.0	2.614	1.0	0.0036	0.219
125	10.5	0.0	0.427	1.0	1.0	0.000	1.0	0.0016	0.040
126	6.5	0.0	8.045	1.0	1.0	1.0	6.115	0.0001	0.214
126	10.5	0.0	0.096	1.0	1.0	1.0	2.594	0.0003	0.037
1234	6.5	0.0	2.125	0.153	0.519	1.0	1.0	0.0001	0.207
1234	10.5	0.0	0.163	0.706	0.330	1.0	1.0	0.0006	0.032
1235	6.5	0.0	10.00	0.361	1.0	5.595	1.0	0.0076	0.207
1235	10.5	0.0	2.582	3.182	1.0	10.00	1.0	0.0138	0.033
1236	6.5	0.0	3.206	0.249	1.0	1.0	1.829	0.0001	0.208
1236	10.5	0.0	0.243	1.714	1.0	1.0	3.380	0.0007	0.032
2345	6.5	1.0	10.00	0.785	0.409	5.629	1.0	0.0059	0.265
2345	10.5	1.0	4.897	4.952	2.202	10.00	1.0	0.0132	0.058
2346	6.5	1.0	10.00	0.944	1.031	0.869	1.0	0.0024	0.268
2346	10.5	1.0	4.573	10.00	7.597	10.00	1.0	0.0111	0.051
3456	6.5	1.0	1.0	10.00	5.079	10.00	10.00	0.0024	0.320
3456	10.5	1.0	1.0	10.00	6.218	10.00	10.00	0.0130	0.050
*234	6.5	0.0*	2.125	0.153	0.519	1.0	1.0	0.0001	0.207
*234	10.5	0.0*	0.163	0.706	0.330	1.0	1.0	0.0006	0.032
*2345	6.5	0.0*	2.074	0.157	0.000	2.441	1.0	0.0001	0.208
*2345	10.5	0.0*	0.406	1.100	0.336	2.707	1.0	0.0023	0.032
*2345	6.5/13 [x]	0.0*	2.462	0.319	0.336	2.981	1.0	0.0001	0.208
*2345	10.5/21 [x]	0.0*	0.100	1.139	0.338	2.673	1.0	0.0007	0.033
*2345	6.5/26 [x]	0.0*	3.656	0.506	0.284	4.567	1.0	0.0001	0.209
*2345	10.5/42 [x]	0.0*	0.000	1.189	0.346	2.792	1.0	0.0004	0.033
*2346	6.5	0.0*	0.904	0.041	0.057	1.0	0.231	0.0002	0.205
*2346	10.5	0.0*	0.535	4.566	2.925	1.0	10.00	0.0014	0.032
*3456	6.5	0.0*	1.0	0.047	0.023	1.536	0.342	0.0001	0.205
*3456	10.5	0.0*	1.0	3.825	1.654	6.294	4.834	0.0039	0.032
*23456	6.5	0.0*	1.801	0.098	0.181	2.529	0.819	0.0001[+]	0.205
*23456	10.5	0.0*	1.145	1.277	0.517	1.031	0.776	0.0001[+]	0.044
1234	19.0	0.0	10.00	0.006	0.000	1.0	1.0	0.0323	0.393
1235	19.0	0.0	10.00	0.042	1.0	0.000	1.0	0.0368	0.399
*2345	19.0	0.0*	10.00	0.005	0.000	0.000	1.0	0.0314	0.389

* Section 1 of the electron energy distribution curve fixed at zero.

[x] The second 'temperature' is that at which the charge exchange PECs are found.

[+] The charge exchange densities ratio is fixed at 0.0001.

and, consequently, these are little more than a label. Essentially, the 312.4Å/289.2Å line intensity ratio should correspond to the values that, in a Maxwellian analysis, would give these temperatures. In the present analysis, the distribution curve was modified by multiplying each section of the curve by a factor, the electron rates calculated and the modelled line intensity ratios determined. Then the position of the peak of the distribution curve was repeatedly adjusted until the appropriate 312.4Å/289.2Å line intensity ratio was obtained. This procedure is repeated varying both the multiplication factors and the charge exchange densities ratio, $n_D n_{g+1}/n_e n_g$, until the RMS of the fractional differences between the five modelled and measured line intensity ratios was minimized using the Constrained_Min IDL routine.

Table 4. Results of the non-Maxwellian analysis, listing fractional differences.

Sections varied	Nominal 'T_e' (eV)	RMS fractional difference	Fractional differences for each ratio				
			420Å/ 312Å	384Å/ 312Å	297Å/ 312Å	289Å/ 312Å	245Å/ 312Å
123	6.5	0.210	-0.42	0.01	-0.05	0.18	0.09
123	10.5	0.038	-0.06	0.01	-0.02	0.03	0.04
124	6.5	0.220	-0.48	-0.06	0.01	0.08	0.07
124	10.5	0.034	-0.06	0.00	0.00	0.04	0.02
125	6.5	0.219	-0.47	-0.08	-0.02	0.09	0.05
125	10.5	0.040	-0.06	0.01	-0.03	0.04	0.04
126	6.5	0.214	-0.45	0.00	0.08	0.12	0.04
126	10.5	0.037	-0.04	0.01	-0.04	0.06	0.00
1234	6.5	0.207	-0.42	0.01	-0.01	0.18	0.06
1234	10.5	0.032	-0.05	0.00	0.00	0.05	0.00
1235	6.5	0.207	-0.41	0.01	-0.05	0.21	0.05
1235	10.5	0.033	-0.05	0.01	-0.02	0.03	0.03
1236	6.5	0.208	-0.43	0.01	-0.01	0.17	0.07
1236	10.5	0.032	-0.05	0.00	0.00	0.05	0.00
2345	6.5	0.265	-0.57	-0.06	0.00	0.13	0.01
2345	10.5	0.058	-0.11	0.00	0.00	0.02	0.07
2346	6.5	0.268	-0.59	-0.05	0.00	0.08	0.07
2346	10.5	0.051	-0.10	0.01	0.00	0.04	0.04
3456	6.5	0.320	-0.53	-0.47	0.00	0.10	0.03
3456	10.5	0.050	-0.09	-0.01	0.00	0.05	0.03
*234	6.5	0.207	-0.42	0.01	-0.01	0.18	0.06
*234	10.5	0.032	-0.05	0.00	0.00	0.05	0.00
*2345	6.5	0.208	-0.42	0.00	0.07	0.19	0.01
*2345	10.5	0.032	-0.05	0.01	0.00	0.05	0.00
*2345	6.5/13 [x]	0.208	-0.42	0.01	-0.01	0.19	0.02
*2345	10.5/21 [x]	0.033	-0.06	0.01	0.00	0.05	0.00
*2345	6.5/26 [x]	0.209	-0.42	0.01	-0.01	0.19	0.01
*2345	10.5/42 [x]	0.033	-0.06	0.00	0.00	0.05	0.00
*2346	6.5	0.205	-0.40	0.01	-0.01	0.21	0.01
*2346	10.5	0.032	-0.05	0.00	0.00	0.05	0.00
*3456	6.5	0.205	-0.40	0.01	0.00	0.22	-0.01
*3456	10.5	0.032	-0.05	0.00	0.00	0.05	0.00
*23456	6.5	0.205	-0.41	0.01	-0.01	0.21	0.01
*23456	10.5	0.044	-0.10	0.01	0.00	-0.01	0.01
1234	19.0	0.393	-0.26	-0.04	-0.46	0.48	-0.51
1235	19.0	0.399	-0.25	-0.08	-0.49	0.49	-0.50
*2345	19.0	0.389	-0.26	-0.03	-0.45	0.48	-0.50

* Section 1 of the electron energy distribution curve fixed at zero.

[x] The second 'temperature' is that at which the charge exchange PECs are found.

Results for some of the minimizations carried out are presented in table 3. It can be seen that various sections of the electron energy distribution curve were varied, as well as the charge exchange densities ratio. In this table the multiplication factors and the charge exchange densities ratio corresponding to the minimum are listed. Additionally, the RMS fractional difference is given and table 4 gives a breakdown of the fractional differences for each ratio. The results include cases in which the minimization varies three or four sections of the electron energy distribution curve, together with the charge exchange densities ratio. Five variables was the maximum number that could be varied without the problem becoming underdefined. One common feature of all the minimizations was that if section 1 of the distribution curve was allowed to vary, the factor for this section at the minimum was always found to be 0. In some cases this factor was, therefore, fixed at 0 and four other sections and the charge exchange densities ratio were allowed to vary. Figure 20 shows the electron energy distribution curves for the case in which section 1 is fixed at 0 and sections 2, 3, 4 and 5 are allowed to vary. It is noted that the section 1 factor being 0 at the minimum was also found to apply to the dataset defined in Paper I.

The charge exchange densities ratio was on the whole found to be small, resulting in contributions of at most ~3% and 0.3% to the intensity of the 312.4Å and 384.1Å lines, respectively. There were a few exceptions at the nominal 'temperature' of 10.5eV, where the contribution to the 312.4Å line was as much as ~17%, but no exceptions were found at the lower nominal 'temperature' of 6.5eV, for which the charge exchange contributions were generally smaller. At the higher nominal 'temperature' agreement was found to within experimental uncertainties, all be it with the extreme and unexpected requirement that section 1 of the electron energy distribution curve should vanish. However, at the lower nominal 'temperature' of 6.5eV certain of the fractional differences were significantly greater than the experimental errors. If section 1 of the distribution curve was included in the minimization the RMS fractional difference was typically ~0.2, with the 419.6Å/312.4Å ratio having a typical fractional difference of 0.40-0.45 and the 289.2Å/312.4Å ratio having differences of up to ~0.2. These results are outside the measurement error bars. Excluding section 1 from the minimization resulted in even higher fractional differences, the RMS value being ~0.25-0.33 and the 419.6Å/312.4Å ratio having differences of ~0.5-0.6.

Since the charge exchange contribution at 6.5eV was small, the charge exchange densities ratio was fixed in some runs to a small value, 0.0001, in addition to the section 1 multiplication factor being fixed to 0. This then allowed the other 5 sections of the electron energy distribution curve to be varied. However, it made little difference to the results. Consideration was also given to the fact that the nominal temperatures were not regarded as being reliable, but were being used to access the charge exchange PECs. Runs were carried out doubling and quadrupling the temperatures at which the charge exchange PECs were determined, but again with no significant change to the results.

Finally some runs were carried out in an attempt to match the discrepancies with the scaled 'temperatures', figure 15 to 19. Three examples are given in table 3 and it can be seen that the fractional differences are even larger than the cases in which the temperatures were not scaled. Further, it is noted that at the higher scaled 'temperature', it was not even possible to find a 312.4Å/289.2Å ratio that matched the ratio corresponding to the required 'temperature'.

A wide range of multiplication factors are found, from 0 to 10, these values corresponding to the constraints used in the minimization routine. Although in each case the results found do appear to correspond to a miniumum, for example being independent of the starting values, such a wide variation casts doubt on them having any physical significance. The only reproducible feature is that the section 1 factor vanishes whenever it is allowed to vary. Even apart from explaining this extreme behaviour, it was still not possible to find agreement

between the measured and theoretical ratios at the lower nominal temperature investigated. It must be concluded that a non-Maxwellian electron energy distribution does not provide a satisfactory explanation of the discrepancies.

b. Line-of-sight averaging in regions of steep gradients

In regions where there are steep gradients such as are found in the plasma edge, the line-of-sight average of a particular parameter can differ significantly from its median value, this depending on the contribution from each section of the profile to the parameter of interest. Zacks (2008) suggested this cause as a possible explanation of the observed discrepancies. At low temperatures, the line intensity ratios are strongly dependent on temperature and it is easily shown that the difference between the line-of-sight average and the median can be significant. The precise distribution function of the contribution from each temperature is uncertain, so in this first analysis no more than the sign of the difference and its approximate relative magnitude is required to match those of the discrepancies.

The discrepancies measured with KT2 and KT4/2 (figures 5 to 9) have been used to investigate this effect in most detail. The parameters describing the straight line fits made to these data are listed in table 5 (table 2 of Paper I). To ensure that the temperature range where this effect is most significant is accessed, the existing range of the atomic data, 1.75 to 129eV, was extended. Although the line intensity ratios are strongly varying with temperature at the lowest temperatures, the variations in the effective collision strengths are weaker; consequently, a small extrapolation of the range to 1.5eV is expected to be reliable. In addition, the range at high temperatures is extended to 140eV, the line ratios being checked to ensure that they were smoothly varying. In fact, these data showed very little change in the range 129 to 140eV, the values at 129eV being adequate to describe the ratios up to 140eV. A low density limit model was used as in section 4a. A check was again made to ensure that the derived line ratios did correspond to those calculated with the full collisional-radiative model using ADAS (Summers 2004), agreement being found to within 2% throughout the temperature range of interest. It is noted that only by including the very lowest temperatures, where the temperature dependence is strongest, are significant discrepancies found. At higher temperatures the dependence is too weak for the line-of-sight averaging to differ significantly from a median value, even when averaging over a wide temperature range.

Table 5. Fit parameters to the discrepancies in the line intensity ratios.

Ratio	Gradient	Constant term	Standard error in the gradient
419.6Å/312.4Å	0.0693	-0.1750	0.0049
419.6Å/289.2Å	0.0710	-0.1966	0.0049
384.1Å/312.4Å	-0.0292	1.0823	0.0028
296.9Å/312.4Å	-0.0156	1.0473	0.0025
244.9Å/312.4Å	0.0423	0.6505	0.0087

In order to make the comparison with the fits of table 5, line intensity ratios were averaged over five temperature ranges. For the present analysis, equal contributions to the emission were assumed throughout the temperature range. The ranges were adjusted until the averaged 312.4Å/289.2Å line ratio corresponded to temperatures of ~11, 12, 13, 14 and 15eV. The averages for the other line ratios were found and compared with the modelled line ratios at the above temperatures. This gives the discrepancies as defined by equation (1), which are

illustrated in figures 21 to 25. Straight line fits are made to the points in these figures and their gradients compared with the gradients from table 5. The comparison is presented in table 6. It can be seen that the directions of the discrepancies and their relative magnitudes do not match. In particular, the line-of-sight discrepancies for the 419.6Å/312.4Å and 419.6Å/289.2Å line ratios have gradients of opposite sign. In contrast, for the discrepancies described in Paper I, reproduced in figures 5 and 6, it can be seen that the discrepancies for these two line ratios are very similar, almost overlaying one another. The same is true for the data presented in section 3, figures 10 and 11. Adjusting the distribution of the contributions to the emission will change the magnitudes of the line-of-sight discrepancies, but will not effect their sign. Consequently, it must be concluded that line-of-sight averaging cannot explain either the discrepancies described in Paper I or those detailed in section 3.

Table 6. Comparison of the gradients of the discrepancies in the line intensity ratios.

Ratio	Observed discrepancy	Line-of-sight discrepancy
419.6Å/312.4Å	0.0693	0.0114
419.6Å/289.2Å	0.0710	-0.0096
384.1Å/312.4Å	-0.0292	-0.0074
296.9Å/312.4Å	-0.0156	-0.0383
244.9Å/312.4Å	0.0423	-0.0464

5. Conclusions

The simplest and most reliable test of the theory which describes the passive line emission from a plasma is to compare the measurements of ratios of spectral line intensities emitted from the same ionization stage. A study has been made of the C emission from the JET plasma edge, which shows that there are discrepancies between the theoretical and measured values. This contrasts with measurements of C IV emission from the JET divertor for which the agreement is limited only by the experimental uncertainties (Lawson *et al*. 2010).

Paper I presents details of an analysis of the C II to C IV emission observed with the JET VUV SPRED survey spectrometer, KT2, and with the XUV Schwob-Fraenkel spectrometer, KT4. This first paper also investigated a number of possible causes for the discrepancy, spectral line blending, the applicability of the steady state approximation, recombination contributing to the electron energy level populations, the accuracy of the atomic data, but no satisfactory explanation was found.

The present paper provides further experimental evidence for the discrepancy, in this case recorded with the divertor viewing XUV/VUV spectrometer, KT7. KT7/2, in particular, is ideal for observing the C IV emission and this spectrometer has a particular advantage for this analysis in that it has a very accurate relative sensitivity calibration throughout the wavelength range of interest. In this case, a clear discrepancy is seen when viewing the SOL just above the throat of the outer divertor. Again, a better understanding of the limitation of the modelling has been sought. In particular, the effect of line-of-sight averaging across plasma regions with steep gradients has been checked and consideration is given to the changes to the electron collisional rates resulting from non-Maxwellian electron energy distributions. Neither of these effects explain the observed discrepancies.

The investigation is to be completed by examining the assumptions made surrounding ionization from the C IV excited levels and from the C III ions to the C IV excited levels. Both of these processes will affect the C IV electron energy level populations

This work was carried out within the framework of the European Fusion Development Agreement and was partly funded by the United Kingdom Engineering and Physical Sciences Research Council under grant EP/G003955 and the European Communities under the contract of Association between EURATOM and CCFE. FPK is grateful to AWE Aldermaston for the award of a William Penney Fellowship, while KMA acknowledges financial support form EPSRC. The views and opinions expressed herein do not necessarily reflect those of the European Commission.
* See the Appendix of F Romanelli *et al*., Proceedings of the 22nd IAEA Fusion Energy Conference, 2008, Geneva, Switzerland.

References

Aggarwal K M and Keenan F P, 2004, Phys. Scr., **69**, 385
Fonck R J, Ramsey A T, Yelle R V, 1982, Appl. Opt., **21**, 2115
Lawson K D *et al*., 2009a (Paper I), JET Report, 'Comparison of modelled C VUV line intensity ratios with observations of the emission from the JET plasma SOL - I'
Lawson K D *et al*., 2009b, JINST **4** P04013
Lawson K D *et al*., 2009c, JET Report, 'A relative sensitivity calibration of the JET KT7/2 spectrometer'
Lawson K D *et al*., 2010, ' An analysis of VUV C IV emission from the JET divertor giving measurements of electron temperatures', To be submitted to PPCF
Maggi C F, 1996, Ph.D. Thesis, University of Strathclyde
Sampson D H, Zhang H L, Fontes C J, 1990, *ADNDT*, **44**, 209
Schwob J L, Wouters A W, Suckewer S, Finkenthal M, 1987, Rev. Sci. Instrum., **58**, 1601
Summers H P, 2004, 'The ADAS User Manual, version 2.6, http://adas.phys.strath.ac.uk'
Whiteford A D, Badnell N R, Balance C P, Loch S D, O'Mullane M G, Summers H P, 2002, *J. Phys. B*, **35**, 3729
Wolf R C *et al*., 1995, JET Preprint, JET-P(95)34
Zacks J, 2008, Ph. D. Thesis, Queen's University, Belfast
Zhang H L, Sampson D H, Fontes C J, 1990, *ADNDT*, **44**, 31

Figure captions

Figure 1. Lines of sight of the JET divertor viewing spectrometer, KT7. — divertor view, — view to SOL above outer divertor throat and — magnetic configuration of pulse 69957 at 10s.
Figure 2. The KT7/2 spectrum for JET pulse 67966 averaged between times 9.3 and 9.4s.
Figure 3. The KT7/2 spectrum for JET pulse 69931 averaged between times 2.3 and 2.6s.
Figure 4. The relative inverse sensitivity calibration (S^{-1} at 312.4Å = 1) for KT7/2. + points derived from the Na- and Li-like ratios, * from C IV ratios. — 2nd order polynomial fit.
Figure 5. Discrepancy (d) for the 419.6Å/312.4Å line ratio measured by KT2 plotted against T_e from the 312.4Å/289.2Å ratio. The line is a straight line fit made to the points +.
Figure 6. Discrepancy (d) for the 419.6Å/289.2Å line ratio measured by KT2 plotted against T_e from the 312.4Å/289.2Å ratio. The line is a straight line fit made to the points +.
Figure 7. Discrepancy (d) for the 384.1Å/312.4Å line ratio measured by KT2 plotted against T_e from the 312.4Å/289.2Å ratio. The line is a straight line fit made to the points +.

Figure 8. Discrepancy (d) for the 296.9Å/312.4Å line ratio measured by KT2 and KT4/2 plotted against T_e from the 312.4Å/289.2Å ratio. The line is a straight line fit made to the points +.
Figure 9. Discrepancy (d) for the 244.9Å/312.4Å line ratio measured by KT2 and KT4/2 plotted against T_e from the 312.4Å/289.2Å ratio. The line is a straight line fit made to the points +.
Figure 10. Discrepancy (d) for the 419.6Å/312.4Å line ratio measured by KT7/2 plotted against T_e from the 312.4Å/289.2Å ratio.
Figure 11. Discrepancy (d) for the 419.6Å/289.2Å line ratio measured by KT7/2 plotted against T_e from the 312.4Å/289.2Å ratio.
Figure 12. Discrepancy (d) for the 384.1Å/312.4Å line ratio measured by KT7/2 plotted against T_e from the 312.4Å/289.2Å ratio.
Figure 13. Discrepancy (d) for the 296.9Å/312.4Å line ratio measured by KT7/2 plotted against T_e from the 312.4Å/289.2Å ratio.
Figure 14. Discrepancy (d) for the 244.9Å/312.4Å line ratio measured by KT7/2 plotted against T_e from the 312.4Å/289.2Å ratio.
Figure 15. Discrepancy (d) for the 419.6Å/312.4Å line ratio measured by KT7/2 plotted against T_e scaled to match the divertor measurements of T_e.
Figure 16. Discrepancy (d) for the 419.6Å/289.2Å line ratio measured by KT7/2 plotted against T_e scaled to match the divertor measurements of T_e.
Figure 17. Discrepancy (d) for the 384.1Å/312.4Å line ratio measured by KT7/2 plotted against T_e scaled to match the divertor measurements of T_e.
Figure 18. Discrepancy (d) for the 296.9Å/312.4Å line ratio measured by KT7/2 plotted against T_e scaled to match the divertor measurements of T_e.
Figure 19. Discrepancy (d) for the 244.9Å/312.4Å line ratio measured by KT7/2 plotted against T_e scaled to match the divertor measurements of T_e.
Figure 20. The non-Maxwellian electron energy distribution function for the minimization in which section 1 is fixed at 0 and sections 2, 3, 4 and 5 are allowed to vary. - - - function and - - -, — 5 x function with a nominal T_e of 6.5eV, - - - function and - - -, — 5 x function with nominal T_e of 10.5eV. The dashed line corresponds to section 0, which has no effect on the C IV line intensities investigated, and the full line sections 1 to 6, which affect the C IV intensities.
Figure 21. Line of sight averaged discrepancy (d) for the 419.6Å/312.4Å line ratio plotted against T_e from the 312.4Å/289.2Å ratio.
Figure 22. Line of sight averaged discrepancy (d) for the 419.6Å/289.2Å line ratio plotted against T_e from the 312.4Å/289.2Å ratio.
Figure 23. Line of sight averaged discrepancy (d) for the 384.1Å/312.4Å line ratio plotted against T_e from the 312.4Å/289.2Å ratio.
Figure 24. Line of sight averaged discrepancy (d) for the 296.9Å/312.4Å line ratio plotted against T_e from the 312.4Å/289.2Å ratio.
Figure 25. Line of sight averaged discrepancy (d) for the 244.9Å/312.4Å line ratio plotted against T_e from the 312.4Å/289.2Å ratio.

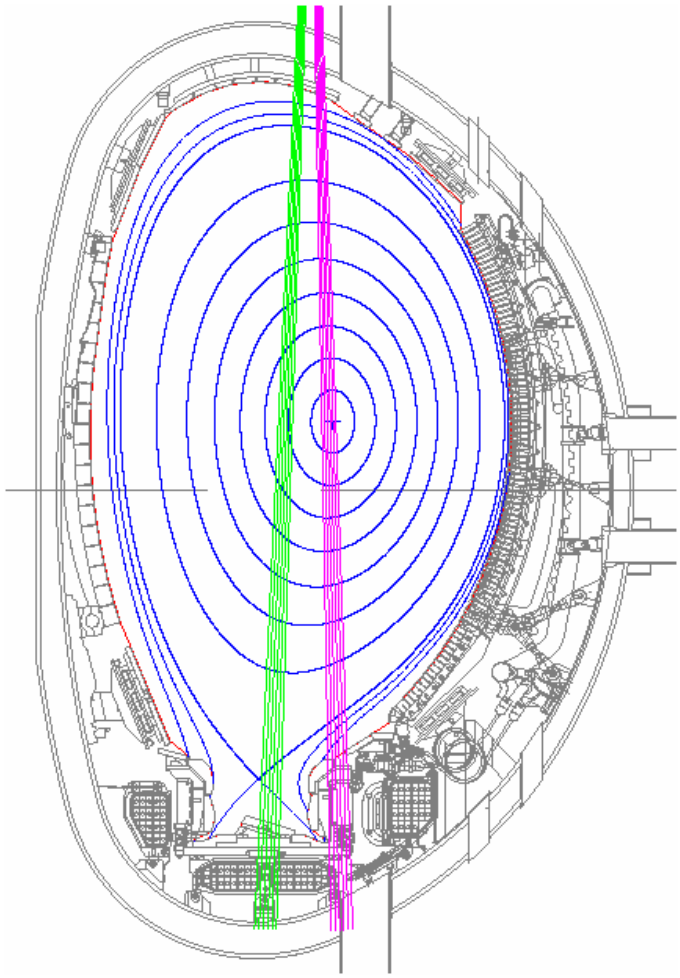

Figure 1.

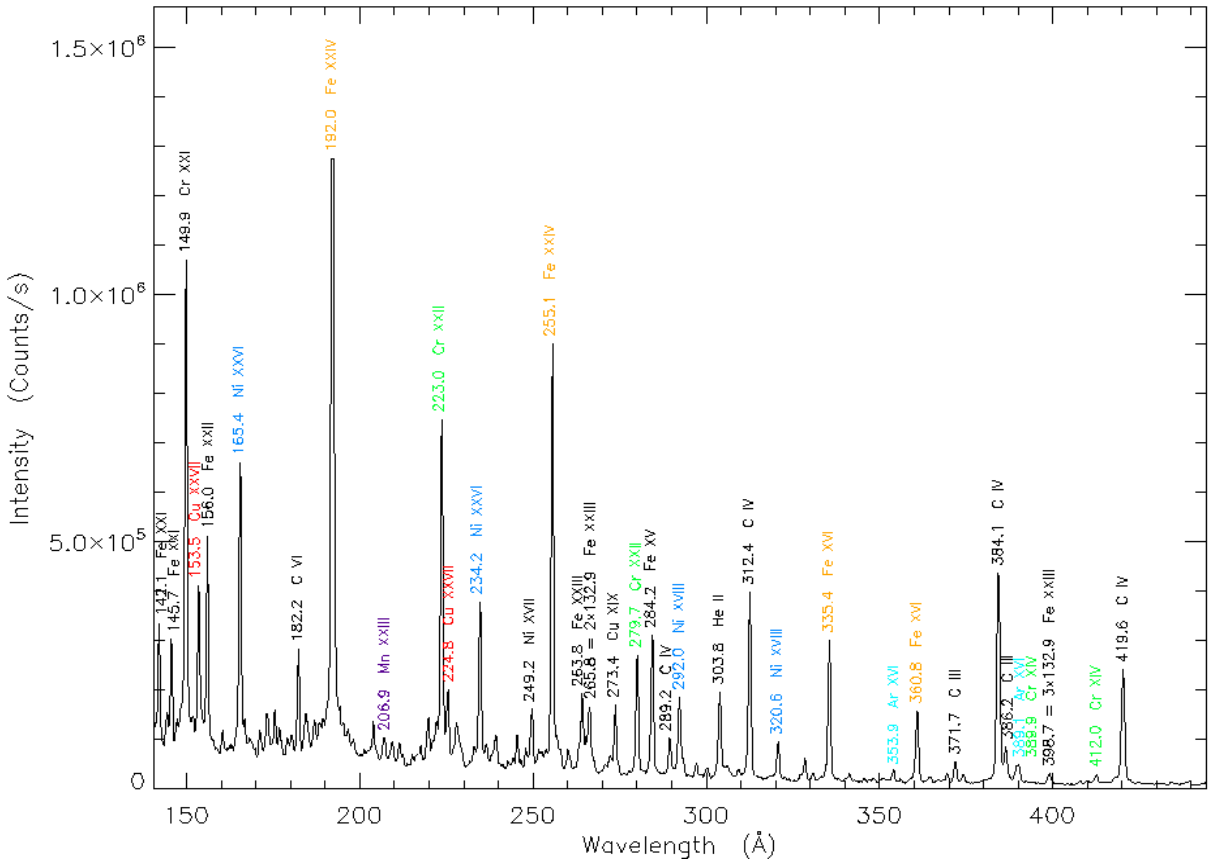

Figure 2.

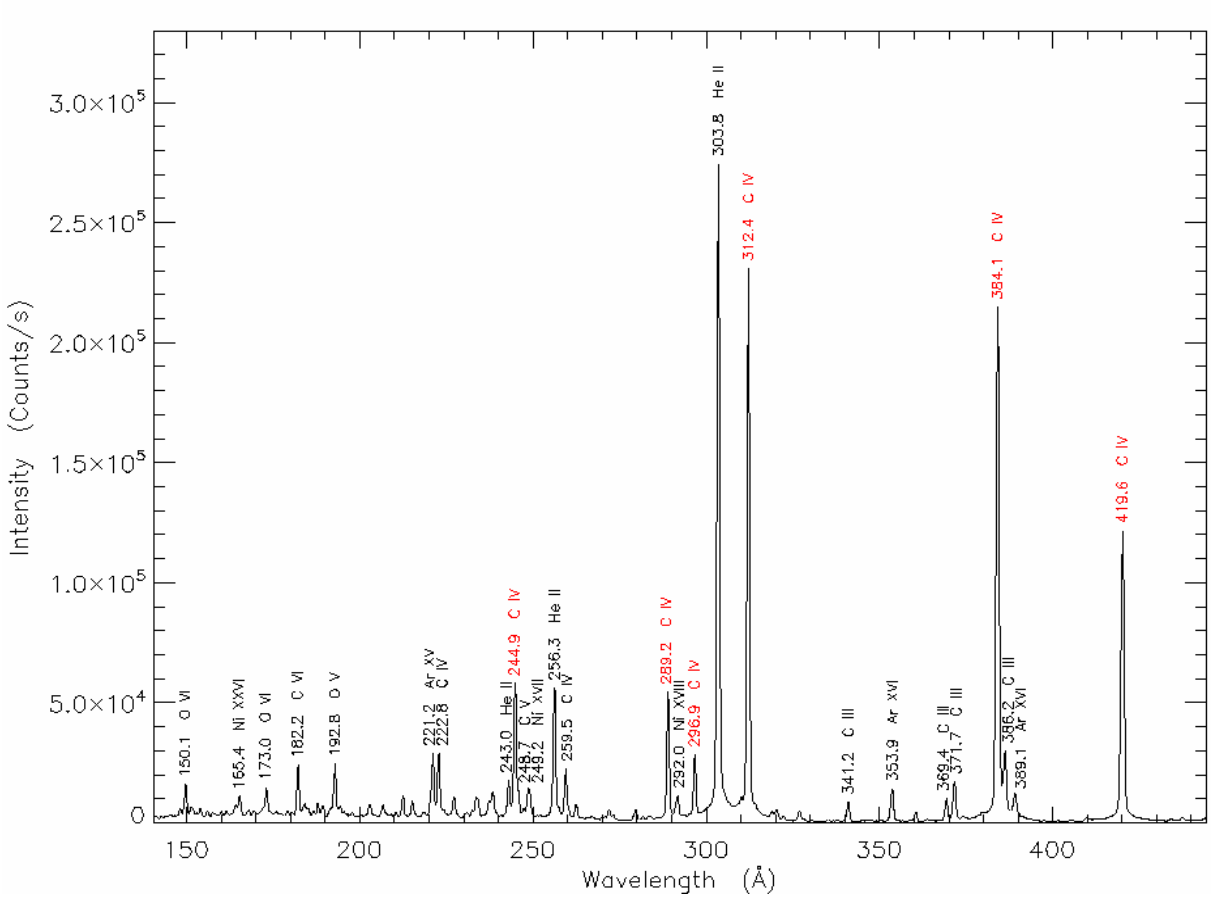

Figure 3.

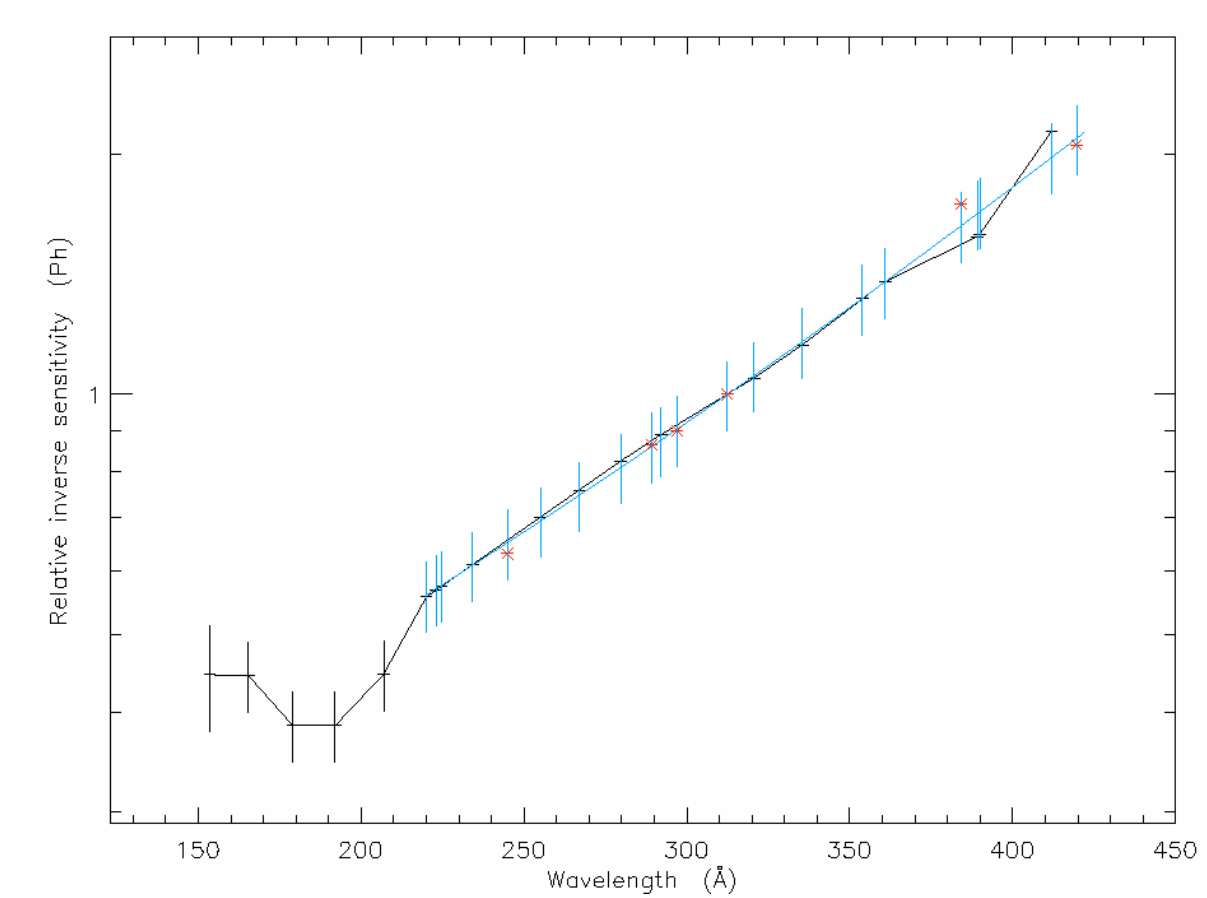

Figure 4.

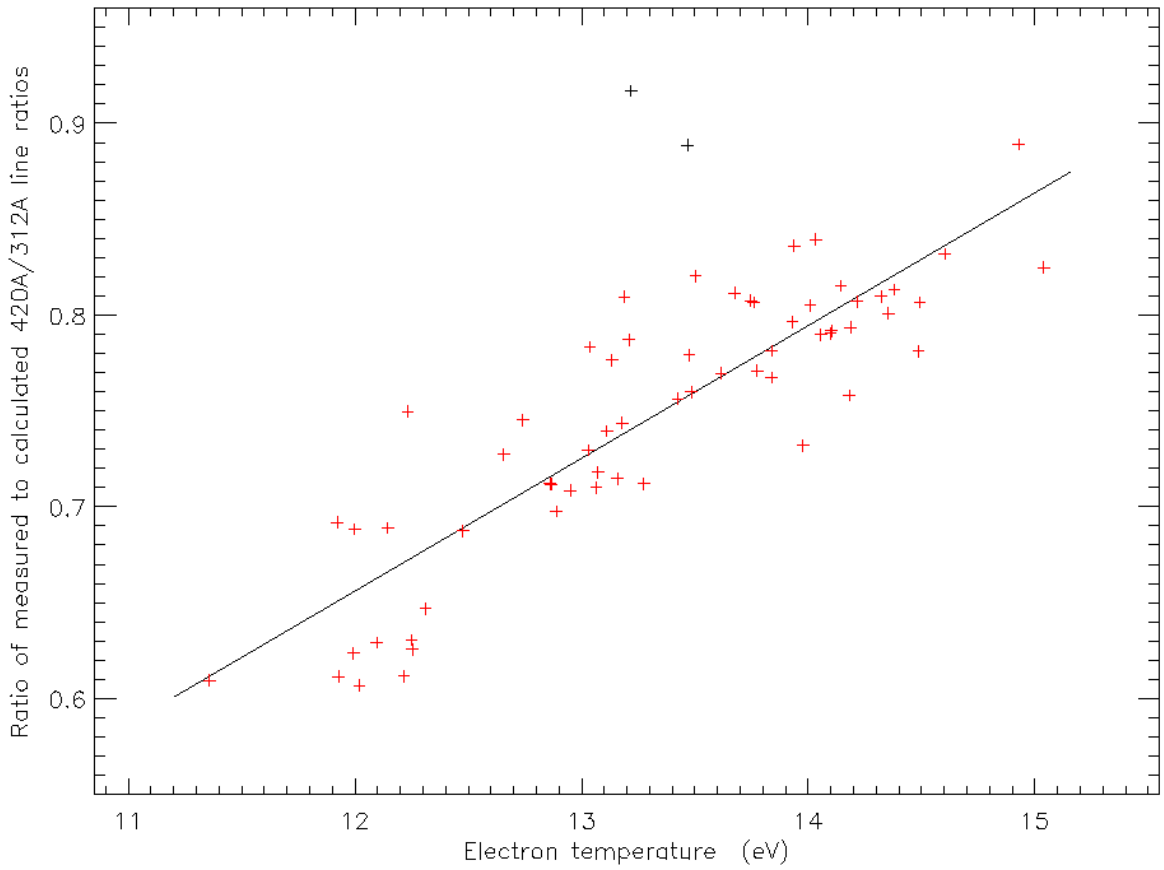

Figure 5.

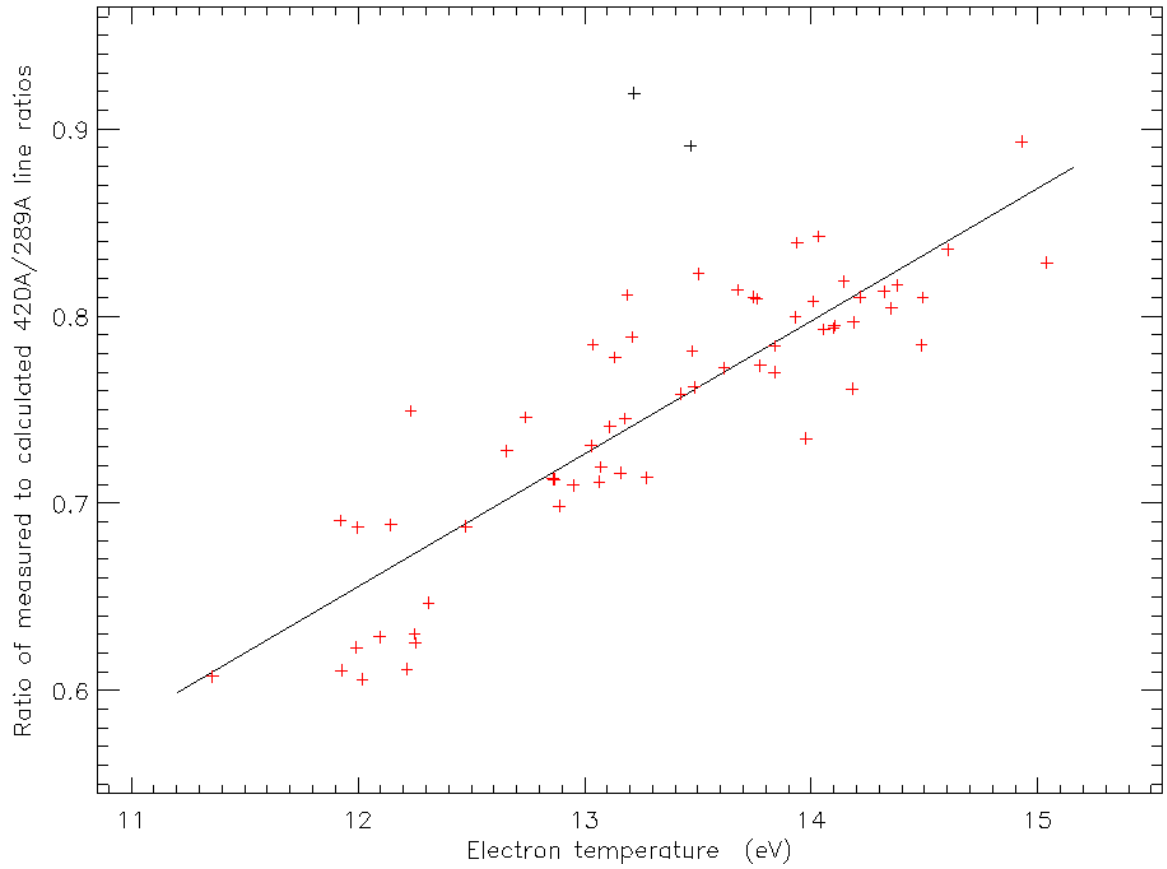

Figure 6.

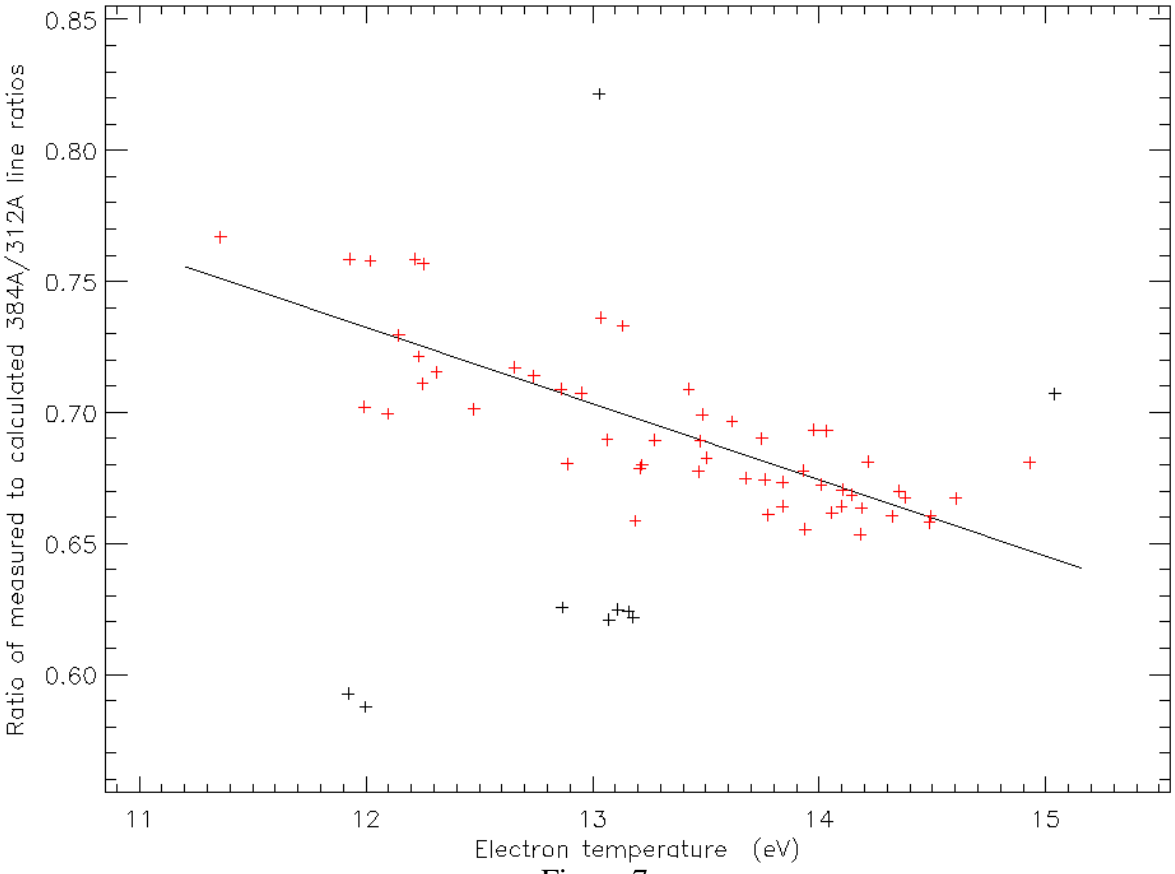

Figure 7.

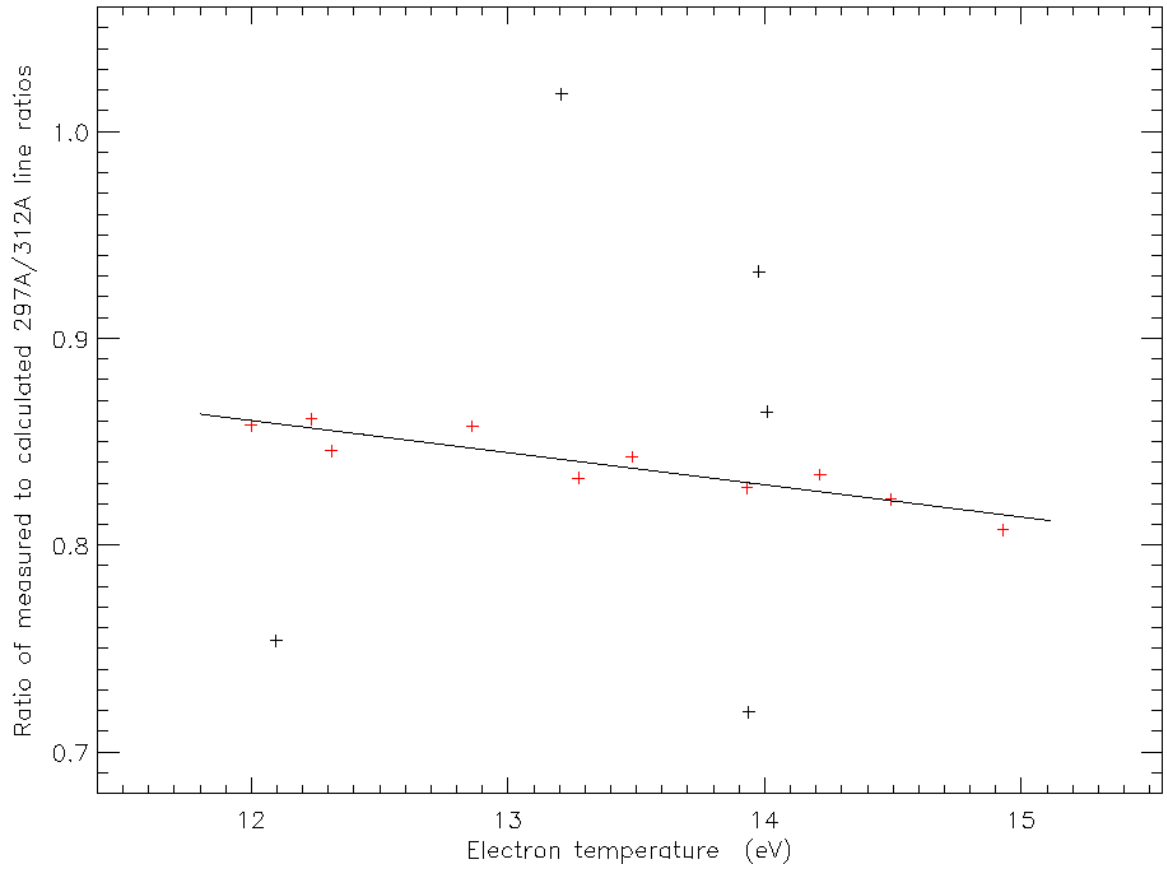

Figure 8.

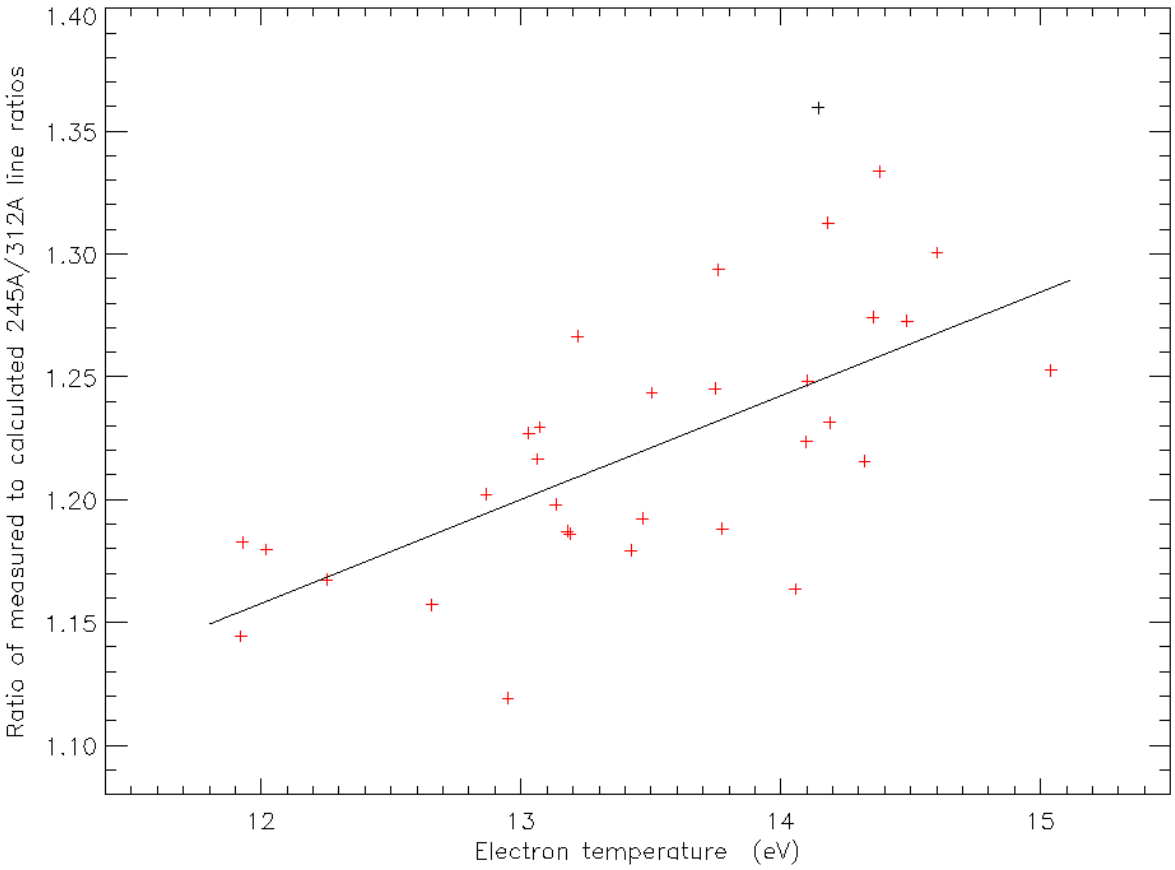

Figure 9.

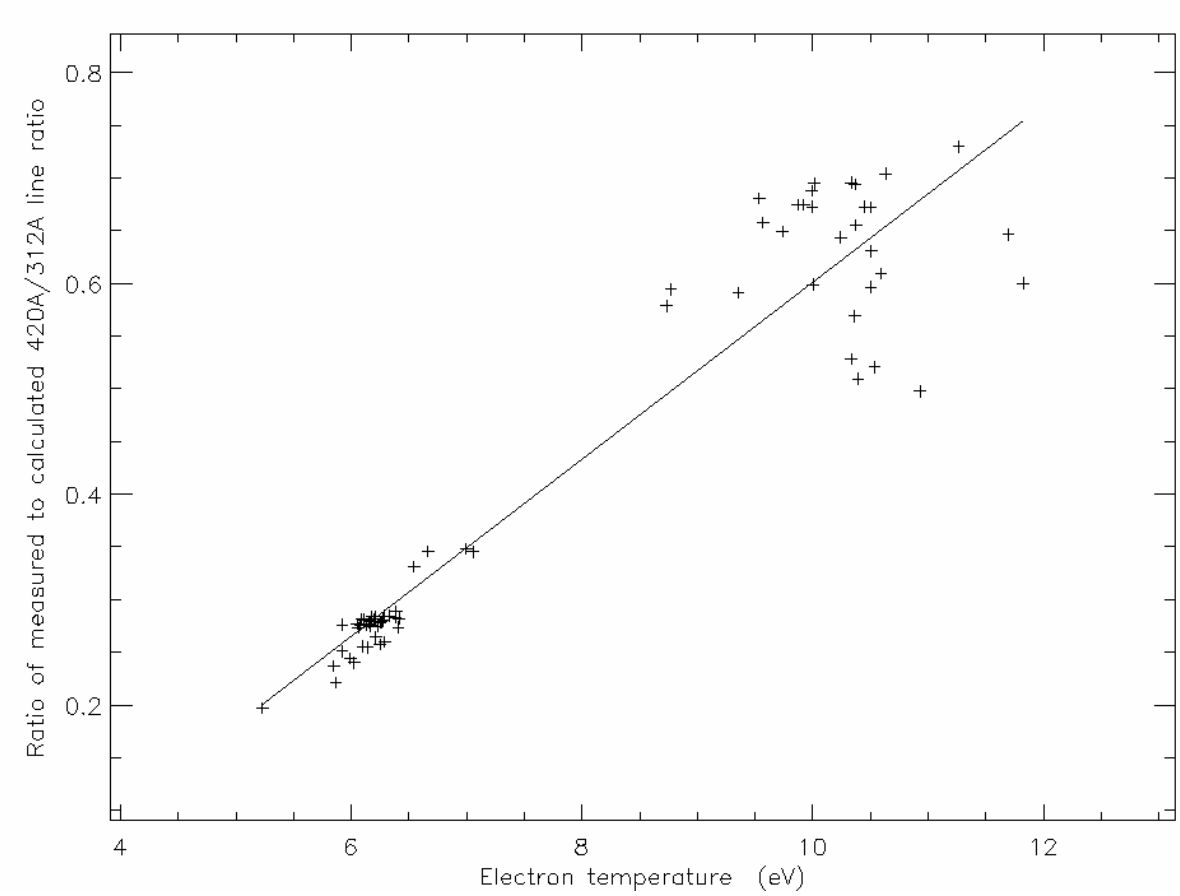

Figure 10.

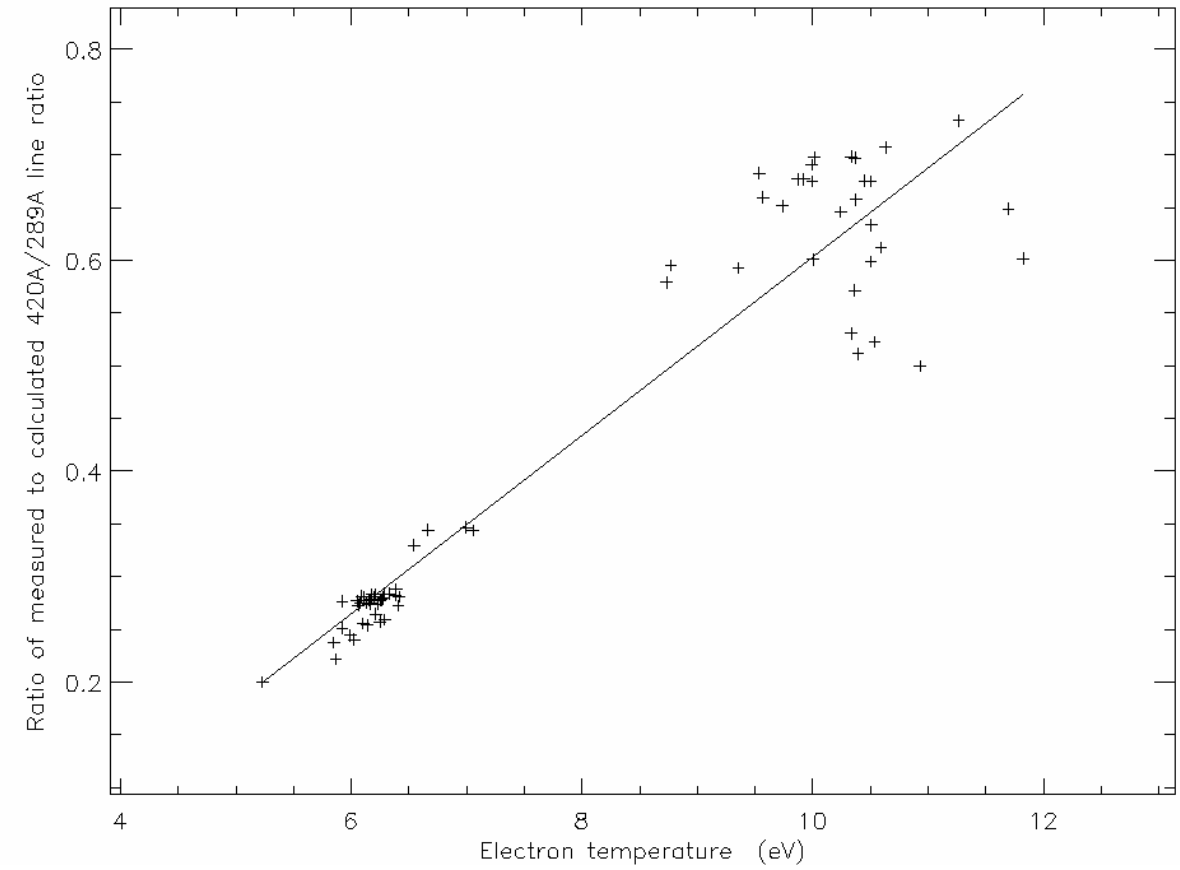

Figure 11.

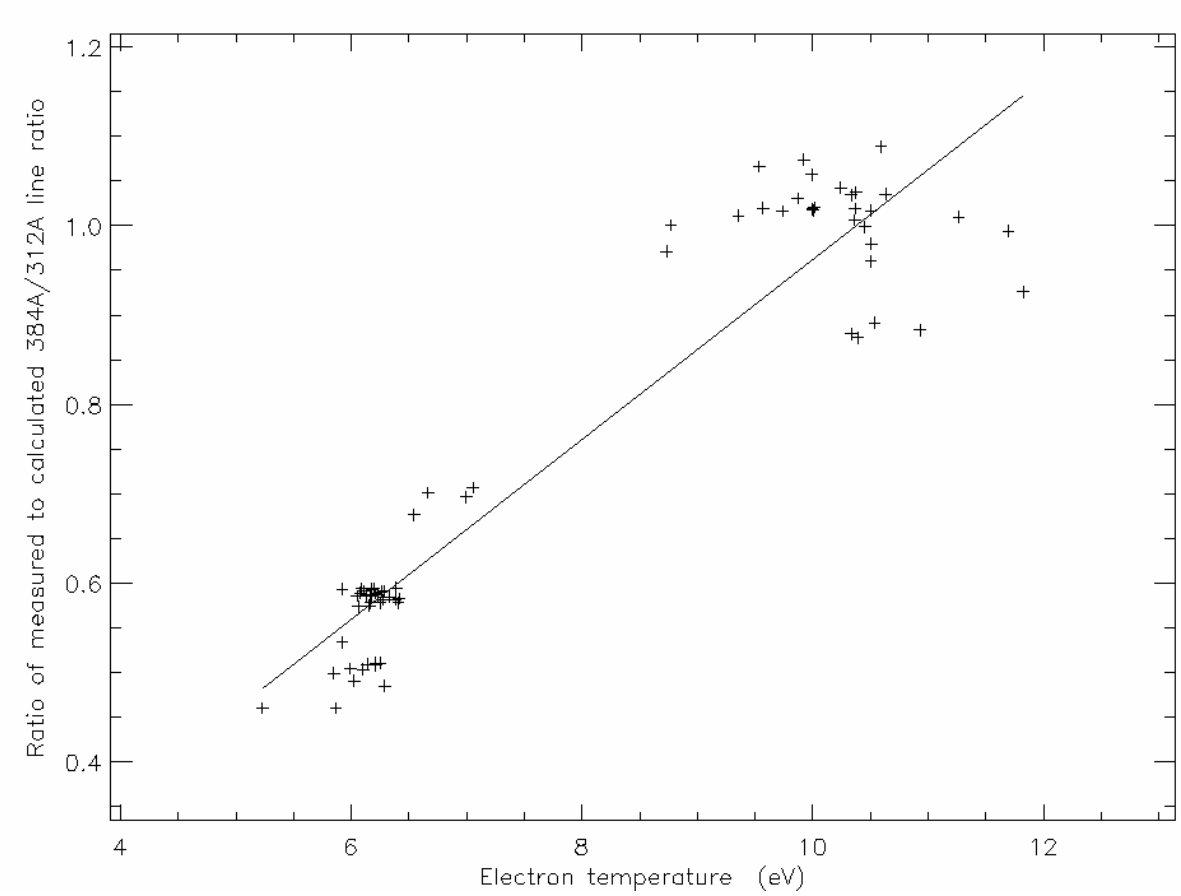

Figure 12.

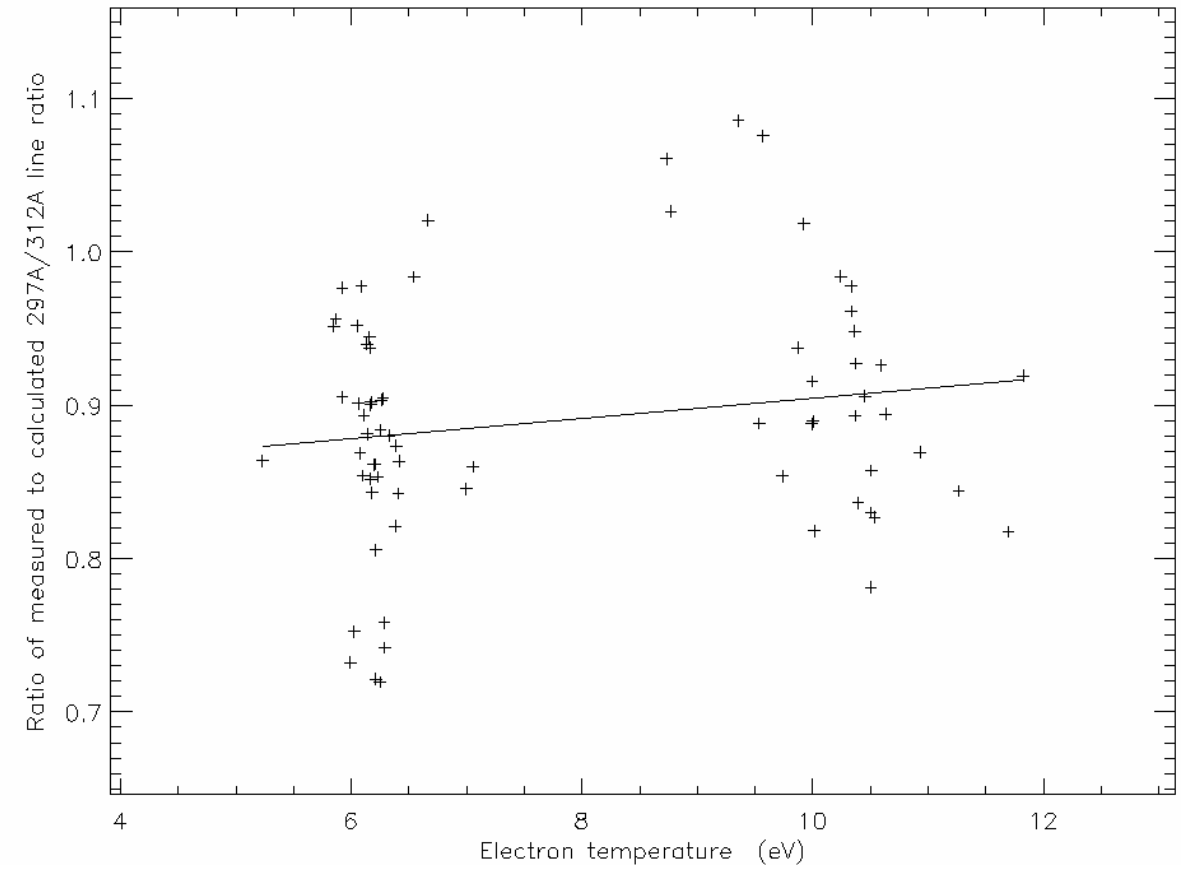

Figure 13.

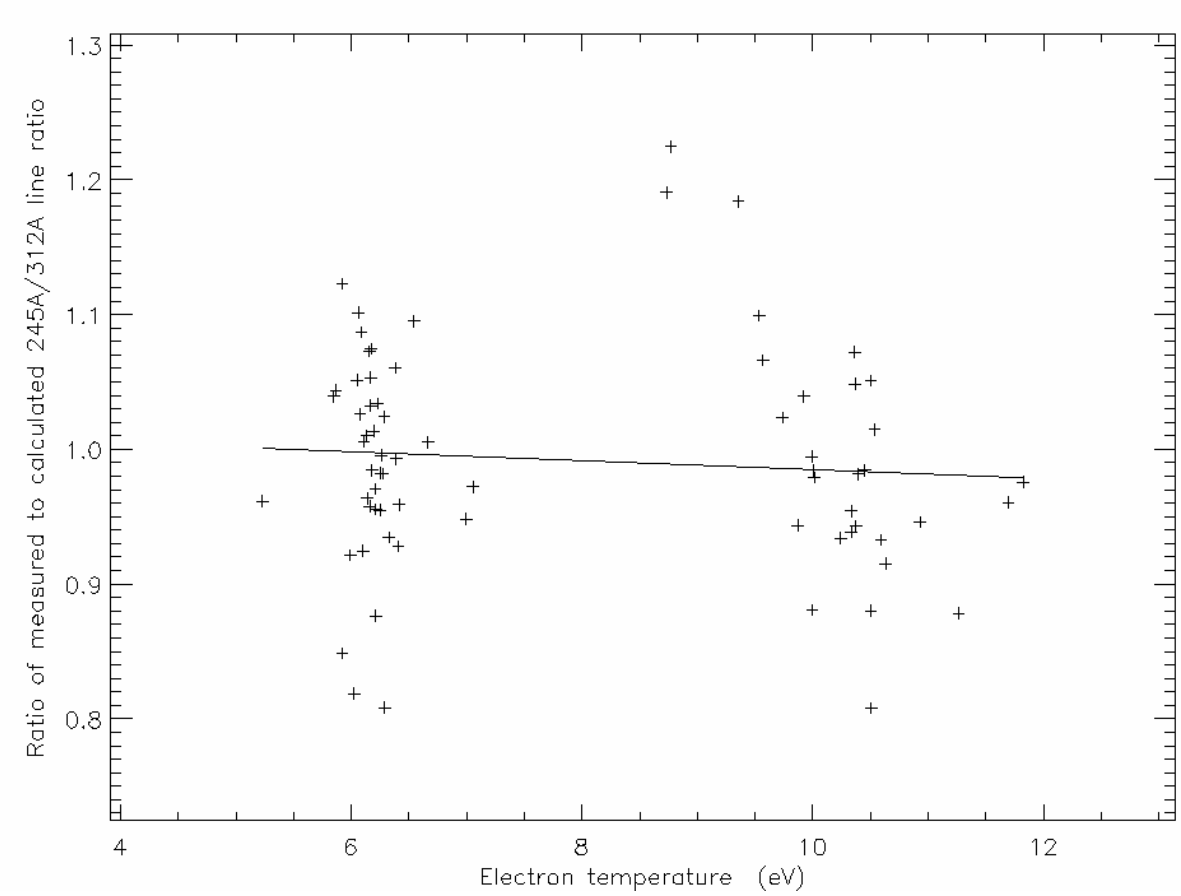

Figure 14.

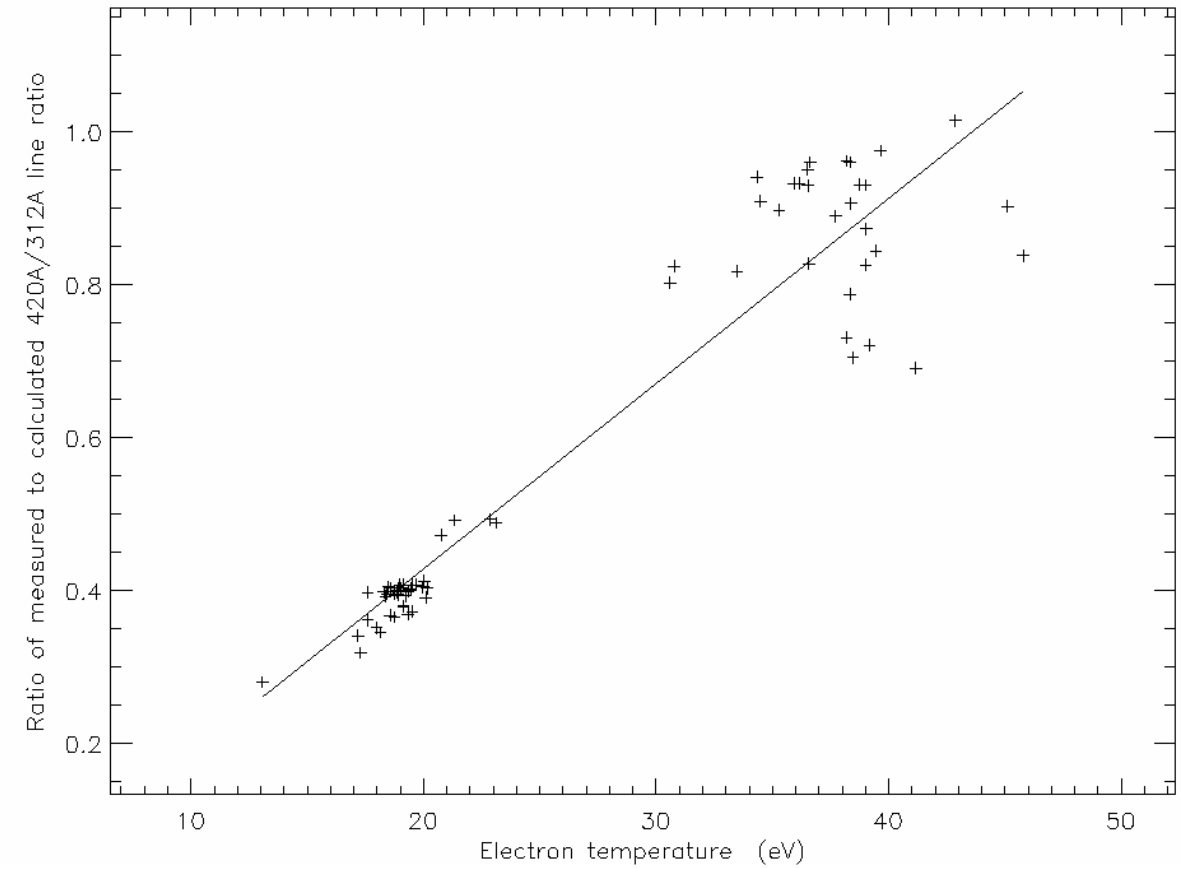

Figure 15.

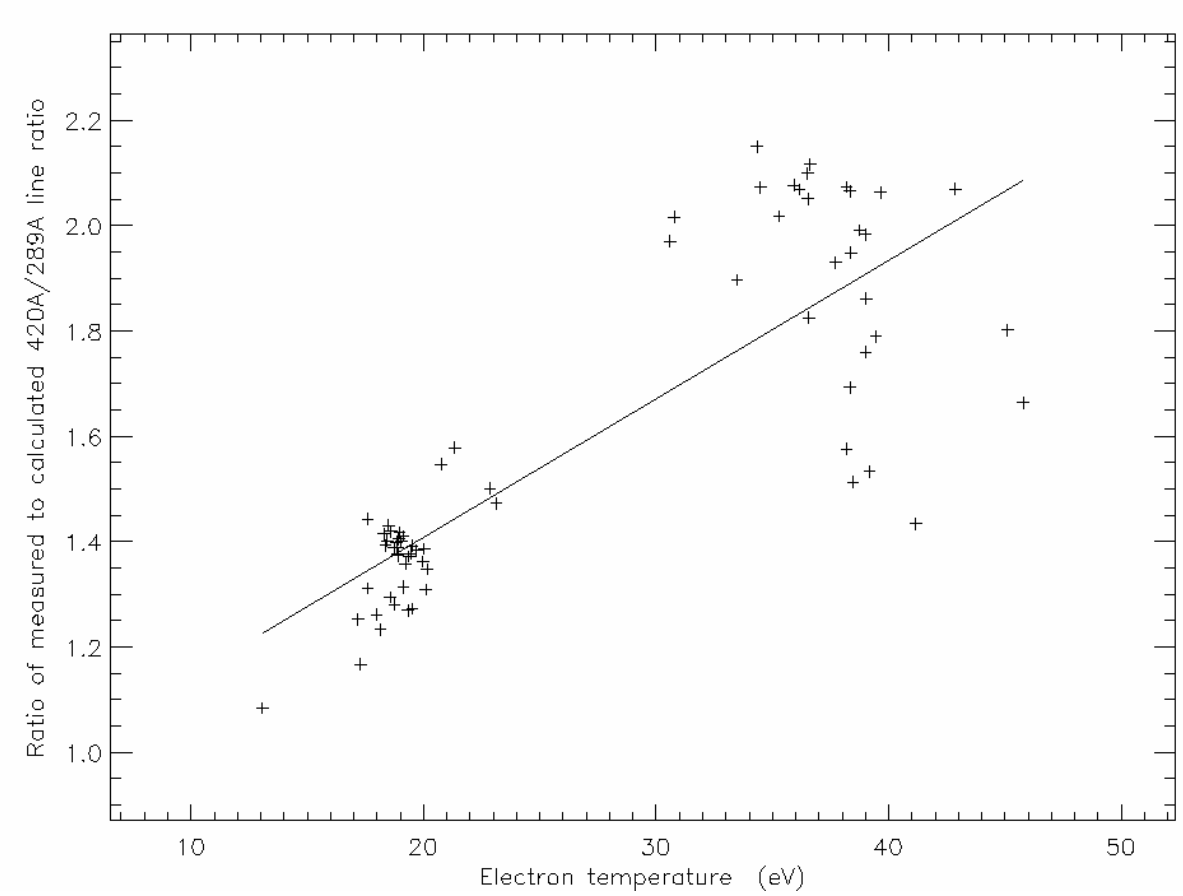

Figure 16.

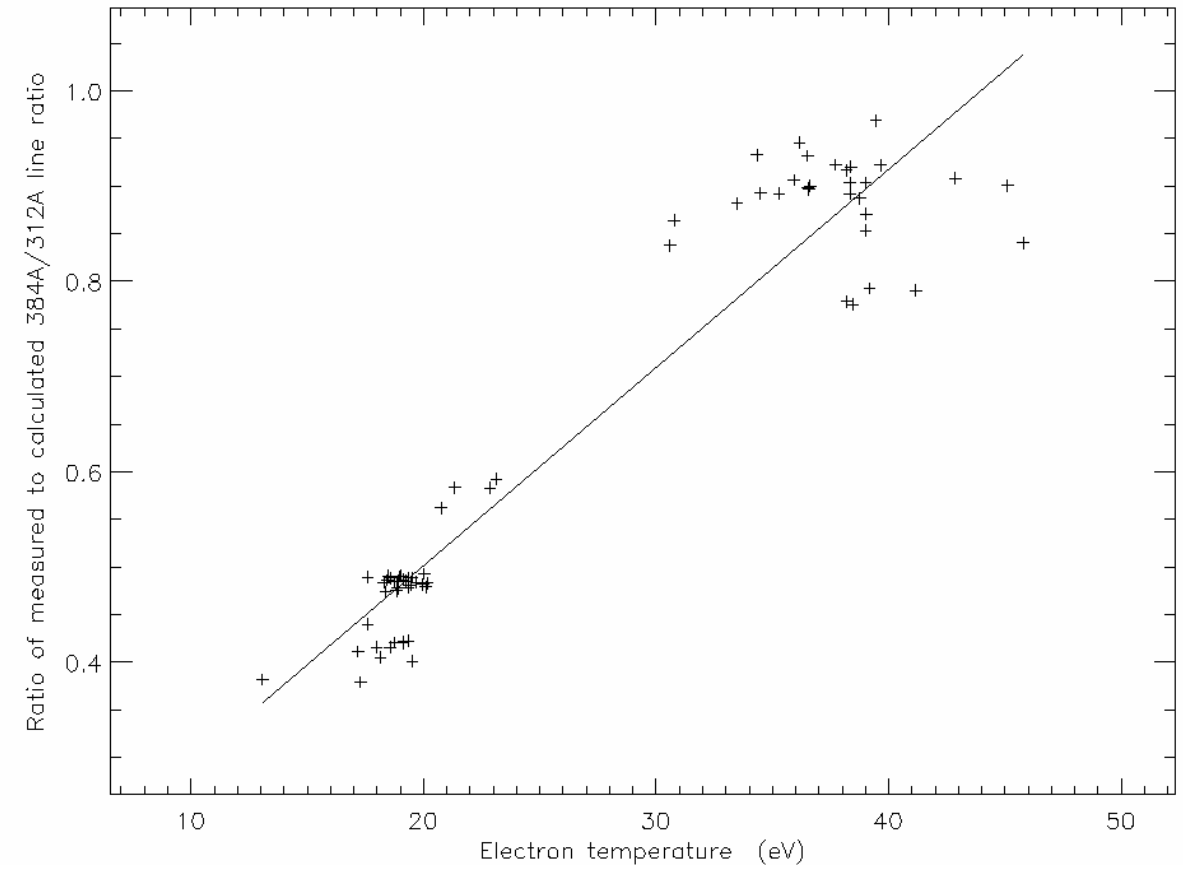

Figure 17.

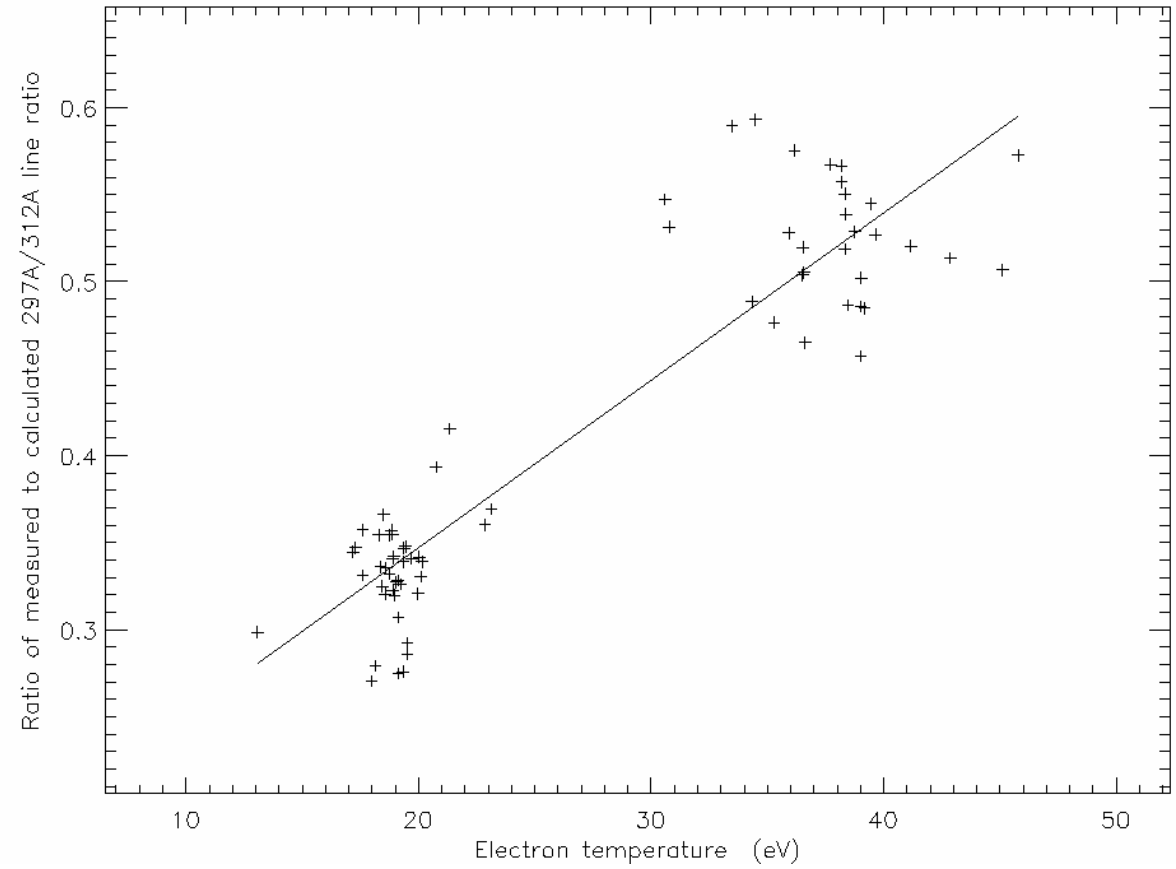

Figure 18.

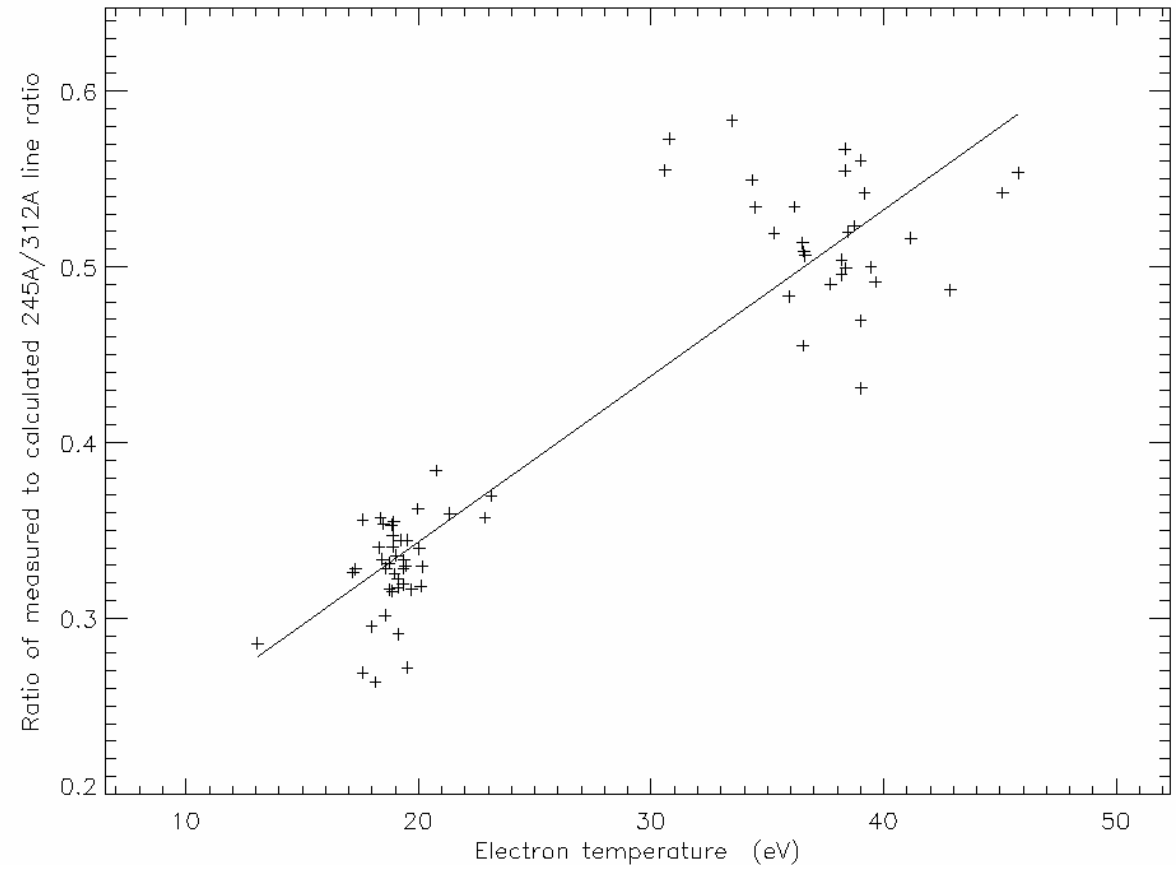

Figure 19.

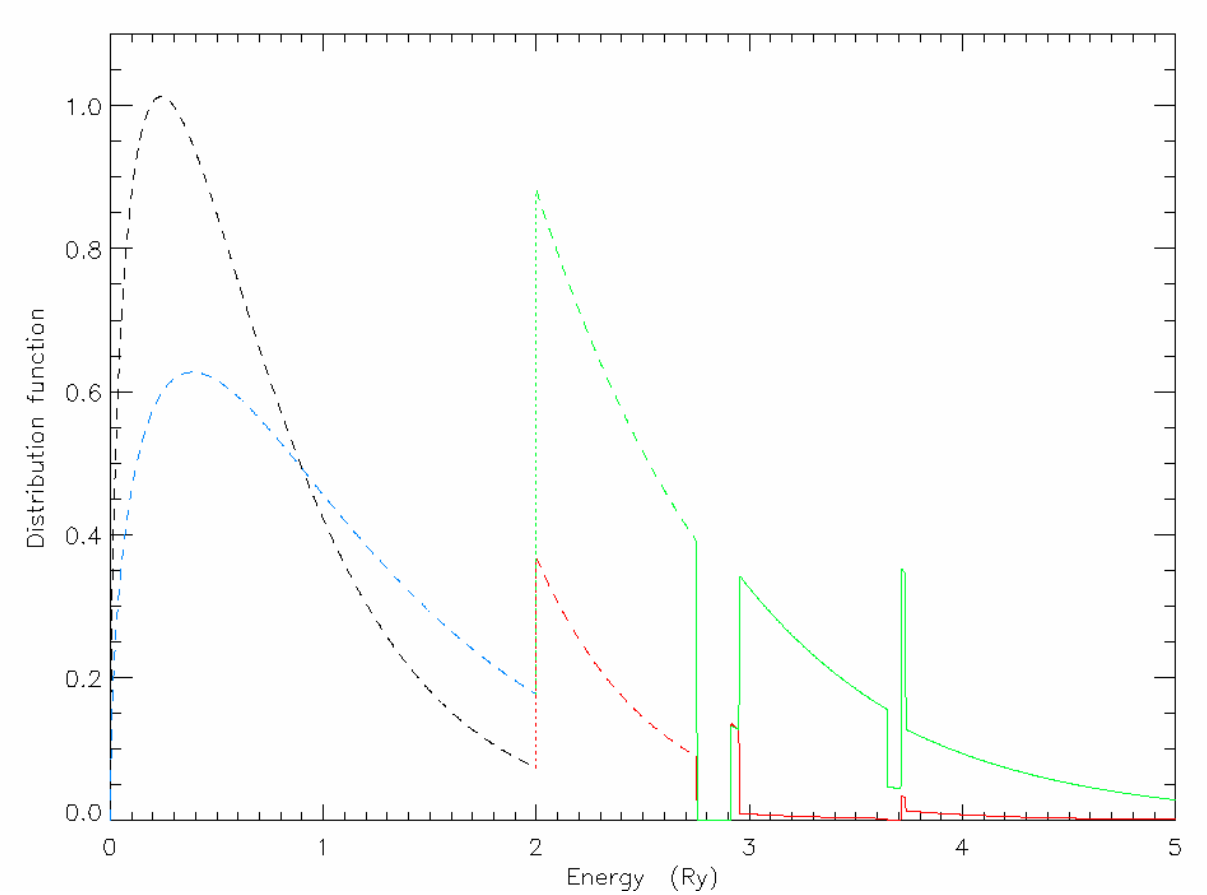

Figure 20.

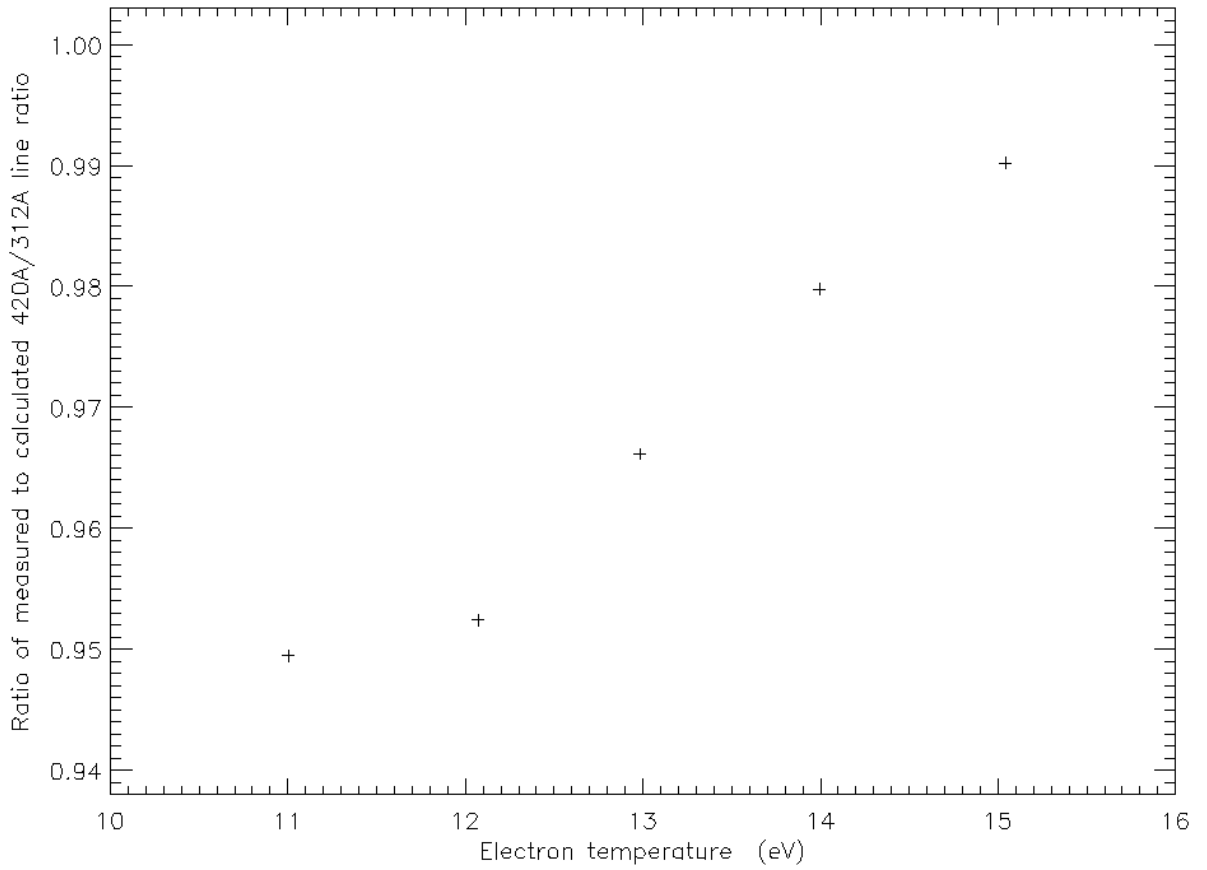

Figure 21.

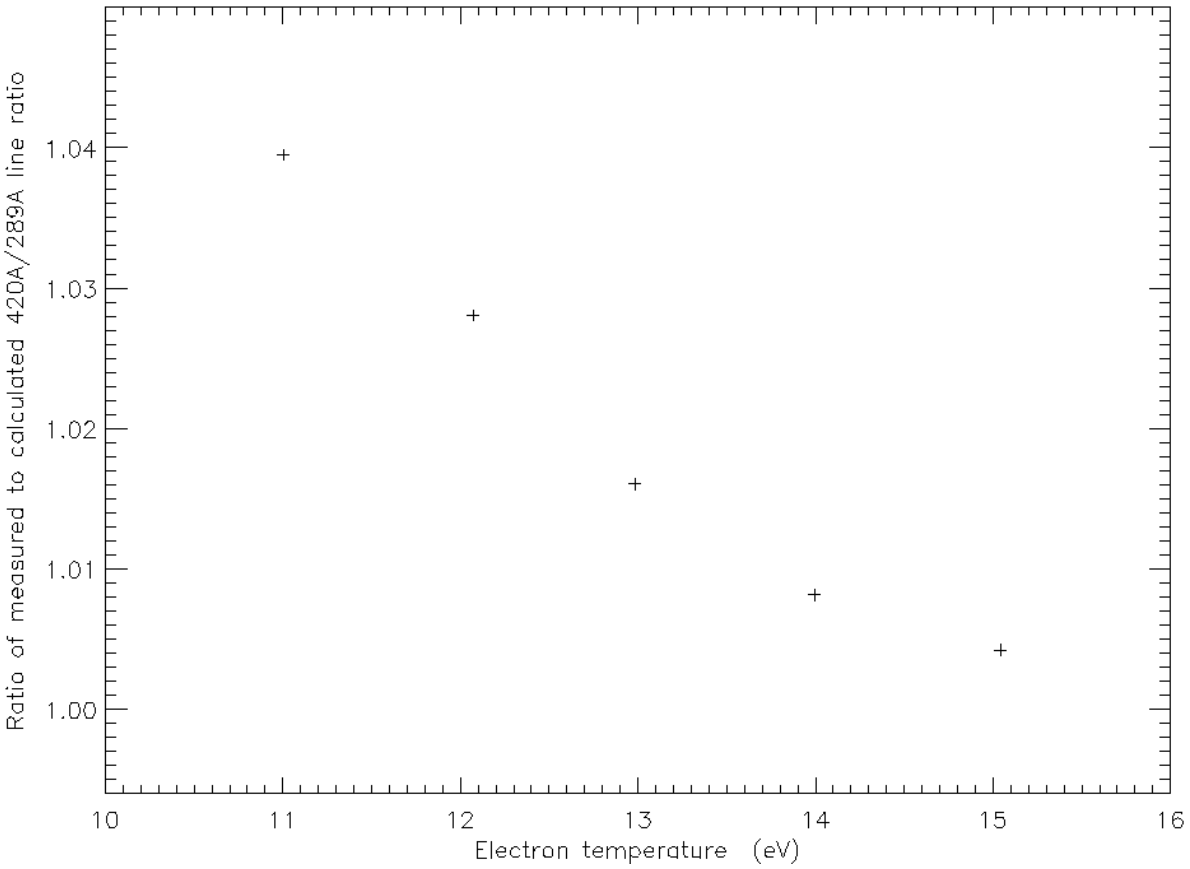

Figure 22.

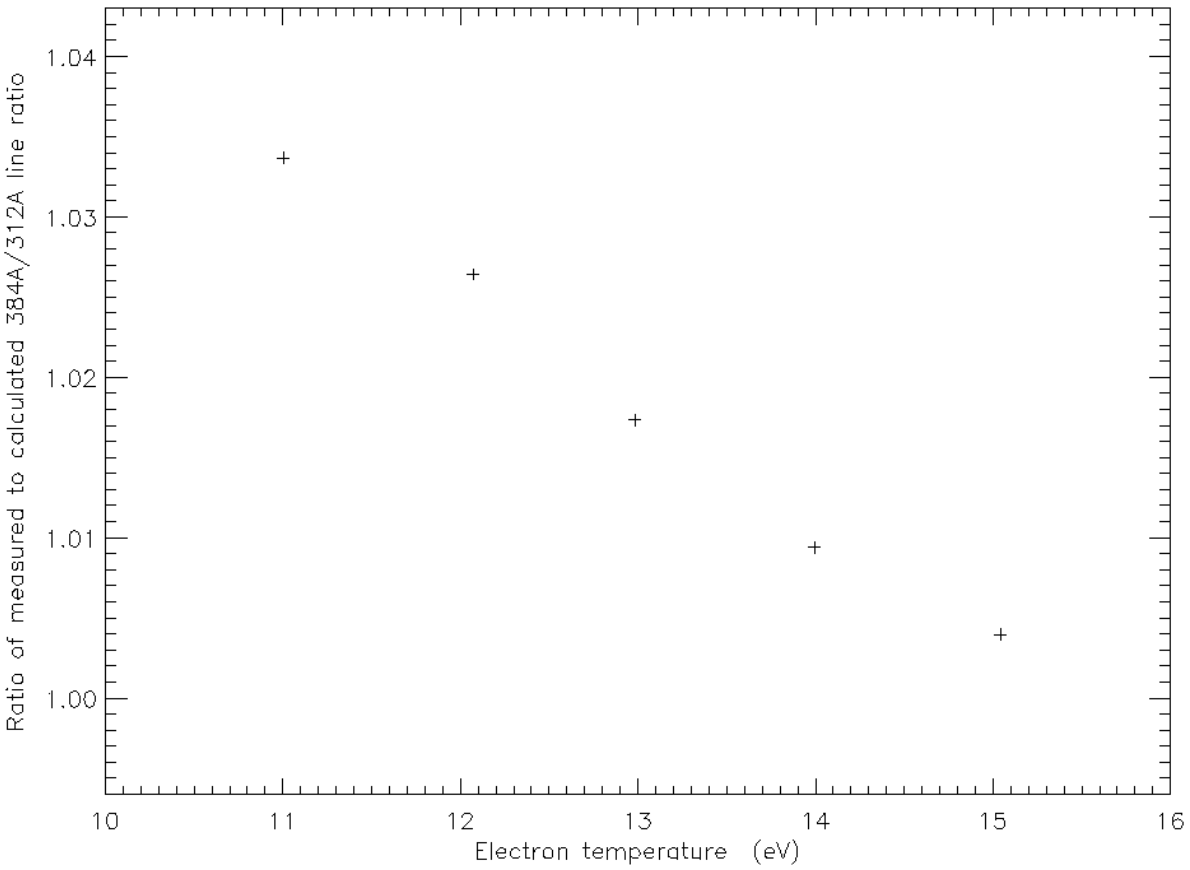

Figure 23.

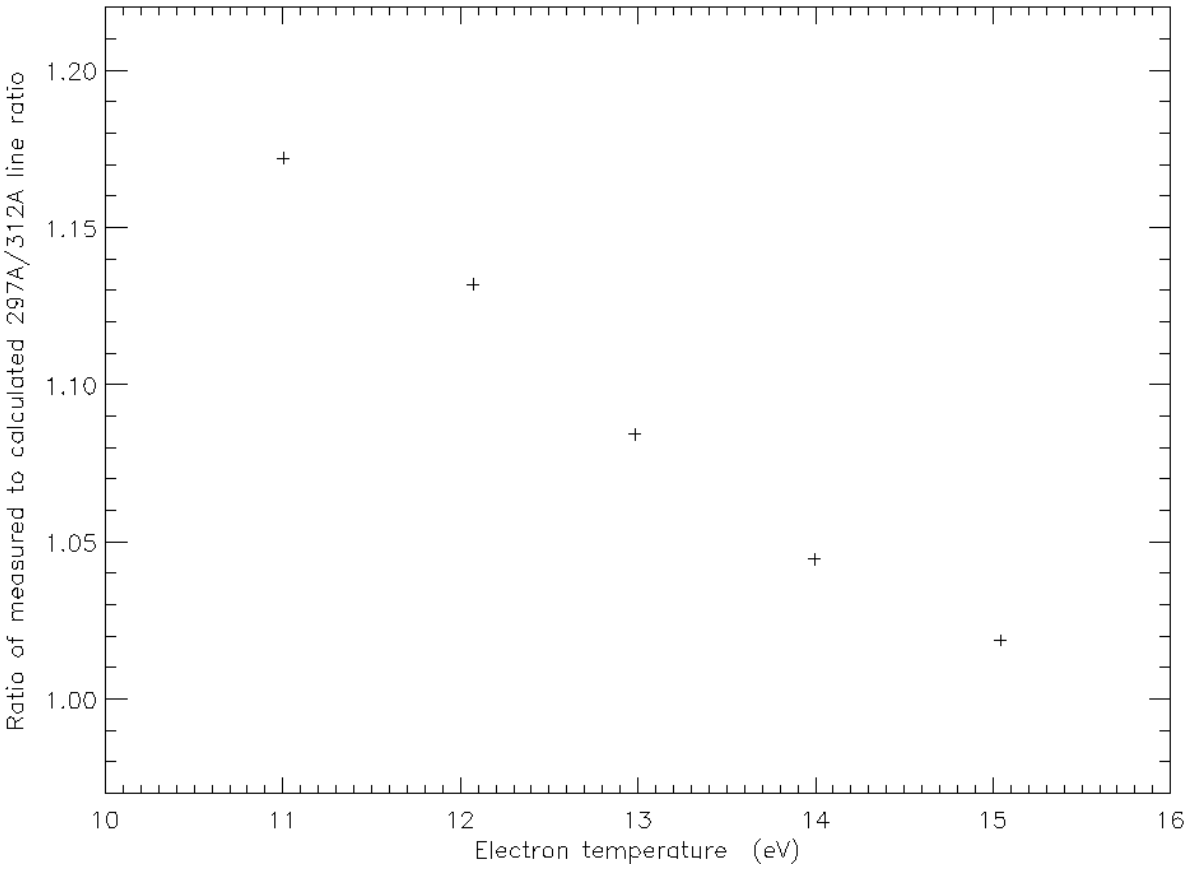

Figure 24.

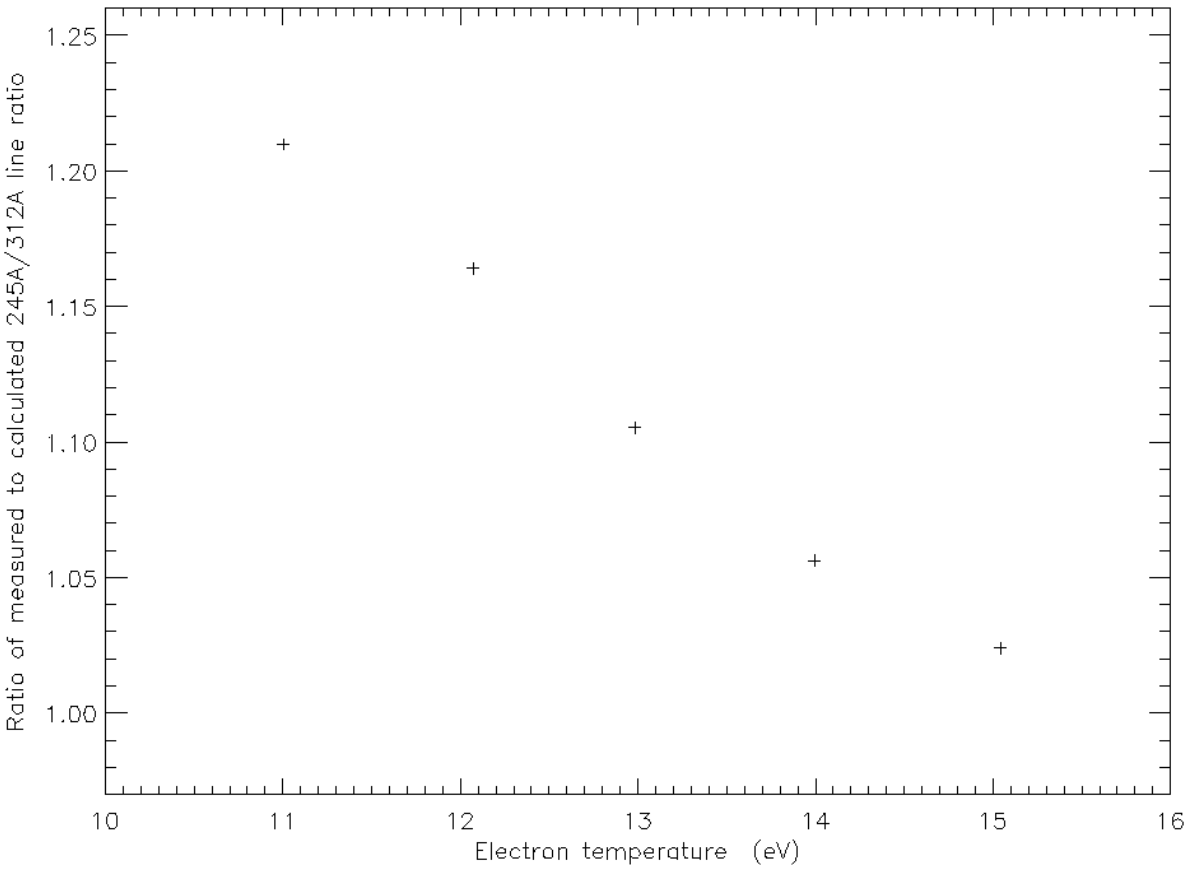

Figure 25.